Submitted to *JGR*
Jan 13,2005

The 1923 Kanto Earthquake Re-evaluated Using a Newly Augmented Geodetic Data Set.

M. Nyst,[1,2] T. Nishimura,[3] F. F. Pollitz,[1] and W. Thatcher[1]

Abstract. This study revisits the mechanism of the 1923 M_s=7.9 Kanto earthquake in Japan. We derive a new source model and use it to assess the accumulation and release of relative plate motion in the Kanto region. We use a new geodetic data set that consists of displacements from leveling and angle changes from triangulation measurements obtained in surveys between 1883 and 1927. Two unique aspects of our analysis are the inclusion of a large number of second order triangulation measurements and the application of a correction to remove interseismic deformation. We evaluate the minimum complexity necessary in the model to fit the data optimally. Our final uniform-slip elastic dislocation model consists of two adjacent 27° dipping low-angle planes accommodating reverse dextral slip of 7.4 m and 6.6 m with azimuths of 145° and 160°, respectively. The geometry of the planes agrees with results from a recent seismic reflection study. The earthquake was located in the Sagami trough, where the Philippine Sea plate subducts under Honshu. Compared to the highly oblique angle of plate convergence the coseismic slip has a more orthogonal orientation to the strike of the plate boundary, suggesting that slip partitioning plays a role in accommodation of plate motion. What other structure is involved in the partitioning is unclear. The time interval necessary to accumulate the 7 m of slip at a plate motion rate of 30 mm/yr agrees with the actual time interval of 220 years between 1923 and the 1703 M_s=8.1 event that ruptured the same plane. However, uplift records of marine coastal terraces in Sagami Bay document 7,500 years of earthquake activity and predict average recurrence intervals of 400 years for events with similar vertical displacement profiles as the 1923 earthquake. This means that the average slip deficit per recurrence interval is about 50% of the relative plate convergence. These findings of plate motion partitioning and slip deficit lead us to suggest that, instead of a simple recurrence model with characteristic earthquakes, additional mechanisms are necessary to describe the accommodation of deformation in the Kanto region. So far, obvious candidates for these alternative mechanisms have not been discovered.

1. Introduction

The M_s = 7.9 1923 Kanto earthquake was one of the most destructive events of the 20th century, causing the deaths of over 140,000 people and destroying Yokohama and large parts of Tokyo. Today, the Tokyo metropolitan area houses more than 30 million people. It accounts for a third of Japan's economy and dominates politics, trade, finance, arts and communication. It is not difficult to imagine that a similar earthquake today would not only cause a human tragedy of immeasurable proportions, but would also have catastrophic effects on the Japanese and world economies. In this paper we adopt a source model that optimally fits a set of geodetic measurements of coseismic deformation and evaluate its implications for earthquake recurrence. To assess the seismic hazard of the Tokyo Bay region, such a model plays a crucial role. First, it has important implications for the derivation of recurrence times of similar earthquakes

[1]U. S. Geological Survey, Menlo Park, USA
[2]Now at Department of Geophysics, Stanford University, Stanford, USA
[3]Geographical Survey Institute, Tsukuba, Japan.

Copyright 2005 by the American Geophysical Union.
0148-0227/05/$9.00

that may be characteristic for this area [*Thatcher,* 1990]. Furthermore, it provides a firm basis for calculating the changes in the static stress field caused by the earthquake and its aftereffects that may have influenced subsequent seismicity [*Harris*, 1998; *Toda et al.* 1998]. In an accompanying paper [*Nyst et al.,* 2004] we address the coseismic stress changes computed with the source model presented here.

The plate tectonic setting of the Tokyo Bay area is complex. The earthquake's epicenter has been located in the Sagami trough [*Ando,* 1971; *Kanamori,* 1971], where the Philippine Sea plate subducts in northwestward direction at an highly oblique angle to the boundary with the overriding northern Honshu block [*Seno et al.*, 1993, 1996; *Heki et al.*, 1999] (Figure 1A). The westward directed convergence of the Pacific plate with respect to northern Honshu is accommodated by subduction of the Pacific plate along the Japan trench. Arc-arc collision north of Izu Peninsula determines the surface deformation west of the Sagami trough [e.g., *Huchon and Kitazato*, 1984; Sagiya et al., 2000]. The two subducting plates meet below Kanto, where seismicity shows that the younger, more buoyant Philippine Sea plate is located above the Pacific plate [e.g., *Ishida,* 1992; *Noguchi,* 2002]. Three-dimensional plate reconstruction requires an elongated contact zone between the two plates with a depth of about 65 km under Tokyo and 55 km under Boso Peninsula and a dip in northwest direction [*Noguchi,* 2002] (Figure 1B).

Early studies of the 1923 earthquake by *Kanamori and Miyamura* [1970], *Kanamori* [1971] and *Ando* [1971, 1974] used seismological and geodetic data to show that the earthquake nucleated in the Odawara region and that the main shock consisted of right-lateral slip with a thrust component on a low-angle fault plane in the Sagami trough (Figure 1C). Subsequent studies, based on geodetic, seismological or geological observations or some combination of them, modeled the source mechanism in more detail. *Matsu'ura et al.* [1980] inverted geodetic data for one and two segment uniform slip source models, which were subsequently refined by *Matsu'ura and Iwasaki* [1983]. *Wald and Somerville* [1995] used the fault plane geometry of the single uniform slip fault model of *Matsu'ura et al.* [1980] to invert geodetic and seismic data to obtain a spatially varying slip model. The approximate geometry and location of the 1923 fault plane as it can be inferred from uplift records of marine coastal terraces [*Ando,* 1974; *Matsuda et al.*, 1978; *Shishikura*, 2003] roughly agrees with the results from geodetic modeling studies.

Like previous studies based on geodetic data we use observations from leveling and first order triangulation measurements that were obtained in campaigns between 1883 and 1927. Unique aspects of the data set in this study are: (1) the use of angle changes rather than displacements, to avoid some major sources of systematic error; (2) the adjustment of the geodetic data for interseismic deformation; and (3) the inclusion of a large number of second order triangulation data that densely sample the Kanto plain. In the first part of the paper we compare the data fit of existing source models and investigate what level of complexity is needed to explain our set of observations. Then we determine the optimum source model. We do not consider seismological observations, because except for two seismograms recorded in Tokyo, only teleseismic observations are available [*Kanamori,* 1971; *Takeo and Kanamori,* 1992] and these have been shown to be of limited value in modeling the coseismic slip [*Matsu'ura,* 1980; *Wald and Somerville,* 1996].

2. Geodetic data

The data used in this study consist of triangulation and leveling data obtained during 2 campaign periods, before and shortly after the 1923 earthquake. In the late 19th century the *Military Land Survey* [1930] of Japan established and surveyed the national geodetic network that consists of horizontal first order control points for triangulation and leveling measurements along roads (Figure 2). At the same time a secondary triangulation network was established to enable a denser spatial sampling of the area. The first and second order triangulation points are separated by about 50 and 10 km, respectively (Figure 3). The second order sites are observed with lower-quality instrumentation and procedures, generally resulting in measurements with larger uncertainties. The first resurveys of these networks were performed in the immediate aftermath of the 1923 earthquake between 1924 and 1931. We exclude geodetic data that were obtained on Izu Peninsula in the first two years after the 1930 $M_s = 7.3$ Kita-Izu earthquake [*Matsuda,* 1972] (Figure 3). Since the surveys, especially the second order triangulation surveys at some sites, span relatively long time intervals of up to 42 years, the geodetic observations include significant interseismic deformation. Under the assumption that the deformation rates before and after the earthquake are similar [*Sagiya and Thatcher,* 1997] we apply corrections using an interseismic deformation model based on continuous GPS measurements made between 1995 and 2000 [*Nishimura and Sagiya,* 2004]. Tables A1 and A2 *in the electronic supplement* list data, data uncertainties determined in sections 2.1 and 2.2 and time span of the measurement, together with the interseismic adjustment computed for each site in section 2.3.

2.1. Triangulation

The initial first order triangulation survey took place between 1891 and 1898. First order post-earthquake surveys were done between 1924 and 1931 [*Military Land Survey,* 1930]. In addition we use the observations from the second order triangulation network that were obtained in a pre-earthquake campaign between 1883 and 1902 and a post-earthquake survey between 1924 and 1925 (Table 1). *Fujii and Nakane* [1983] use this second order triangulation data set in their study of the crustal strain field in Kanto, but it has never been previously used in studying the Kanto earthquake.

Two general approaches exist to use triangulation data for the determination of surface deformation. Previous geodetic studies of the Kanto earthquake are all based on the same method. A reference frame is constructed from several triangulation sites that are assumed to have remained stable during the period of observation. The coordinates of all sites are explicitly determined at each epoch with respect to this reference frame and then displacement vectors are computed from the difference in station position [e.g., *Bibby*, 1981; *Walcott*, 1984]. *Muto* [1932] converted the first order triangulation data into a displacement data set that formed the basis for the early models of *Ando* [1970, 1974]. *Matsu'ura et al.* [1980] show that movement of the reference system defined by *Muto* [1932] causes a systematic error in the displacement field. They removed this artefact by choosing a more stable reference frame. Later models by *Wald and Somerville* [1995] and *Pollitz et al.* [1996] are based on the displacement vector set of *Matsu'ura et al.* [1980]. Another source of error in this method, one that is impossible to remove completely, is the unavoidable propagation through the network of measurement errors at

individual stations. To avoid reference frame problems and to minimize the influence of systematic errors, we choose to apply an alternative method that uses the difference between repeated angle observations as a measure of relative deformation of the network [*Frank*, 1966; *Savage and Burford*, 1970; *Thatcher*, 1975; *Yu and Segall*, 1996]. A disadvantage of this approach is that we can only use repeated angle observations instead of all measurements. Figure 3 shows the triangle network in which the angles were observed at least twice. Because none of the angles between Oshima Island and Japan's mainland were repeated before and after 1923 our data set does not contain information on the deformation across Sagami Bay, and the number of first order data used in this study is somewhat smaller than in to previous studies. However, due to the inclusion of second order data the spatial density of our data set is considerably higher. Our final triangulation data set consists of 31 first and 435 second order repeated angle observations. The largest angle changes were measured in the southwestern part of Boso Peninsula, in Miura Peninsula and along the coast of the Odawara region. The first order angle change data clearly represent a coseismic deformation field of NW-SE oriented extension and to a lesser degree shortening in a NE-SW direction. Although the second-order angle changes provide a shorter wavelength mapping of the coseismic deformation, the overall trend shows NW-SE directed extension west of the Tokyo Bay and NNW-SSE to NNE-SSW oriented extension on Boso Peninsula.

In determining the accuracy of the triangulation measurements we use the method of triangle closure [e.g., *Bomford,* 1980; *Yu and Segall*, 1996]. The measurement error or triangle closure

$$\delta c = \alpha + \beta + \gamma - (180 + \phi_e) \tag{1}$$

is the difference between the sum of the observed angles in a closed triangle, α, β and γ and 180° plus the spherical excess ϕ_e. The spherical excess is given by $\phi_e = mab \sin C$, with a and b the lengths of the two sides opposite to angles α and β, respectively, C is their included angle and m is a factor which depends on the latitude. Following *Bomford* [1980] an estimate of the average observational error, ϵ_a, in a network with N closures is then:

$$\epsilon_a = \sqrt{\frac{\sum_{i=1}^{N} (\delta c)^2}{3N}} \tag{2}$$

We consider all angle measurements of closed triangles for campaigns between 1883 and 1931 in the area of central Honshu that encompasses the Kanto district. The size of the triangle closures of both data sets is randomly distributed, closures sample the region evenly and both first and second order closures are normally distributed, as illustrated by Figures 4A and B. Therefore, we assume that we can safely adopt a simple average error for the triangulation observations in our modeling calculations. Average observational errors for the first and second order triangulation networks range between 0.79-0.83 and 1.23-1.31 arcsec, respectively (Table 1). The value for the first order network is consistent with the estimate of 0.7-1.2 arcsec by *Sagiya and Thatcher* [1999] for first order angle change observations at the Nankai Trough between about 1890 and 1950. As reported elsewhere [Japan Association of Surveyors, 1970] the average error of the second order data is surprisingly small. Because comparison of the average error before 1923 and after 1923 for first

and second order networks shows no large differences, we use 0.82 arcsec for the first order observations and 1.23 arcsec for the second order triangulation observations.

2.2. Leveling data

The leveling measurements were obtained from first order double-run leveling surveys of the 10 routes shown in Figure 5 during two campaign periods. The average length of one first order leveling section is around 2 km long. The pre-earthquake leveling surveys took place between 1891 and 1918. Post-earthquake data were collected between 1923 and 1930 [*Military Land Survey,* 1930] (Table 2).

In double-run surveys the routes are leveled in both directions. Leveling error accumulates with the square root of distance along the route, expressed as $\alpha\sqrt{L}$, where α (in $mm/\sqrt{km}$) is calculated from differences between forward and backward measurements along a first order route and L (in km) is the section length. First order surveys only allow for a maximum discrepancy, the field tolerance factor β (in $mm/\sqrt{km}$), between forward and backward runs of each double-run section. If this field tolerance is not met (i.e. if $\alpha \geq \beta$), the section must be rerun until the forward and backward runs agree to within the tolerance (see also *Marshall et al.* [1991]). Since 1955, the Geographical Survey Institute (GSI) has officially released a standard annual average for α. Errors in earlier surveys need to be determined on a case-by-case basis, which gives rise to several problems. First, it is extremely time-consuming to input all data for forward and backward measurements and then calculate the measurement errors or circuit misclosures. In addition, some of the original notes are missing and existing notes can be difficult to understand, because of rough handwriting or the poor physical quality of these old field notes. Since the observation method of leveling has not changed very much since its introduction to Japan, we determine the data errors in a pragmatic, approximate way. We divide the time interval between 1880 and 1945 into two periods and determine an average error for each period. The first period is from 1880 to 1923 following the Kanto earthquake. The second is from 1924 to 1945, the end of World War II. We digitize the height differences of forward and backward measurements of a number of random sections measured in the Kanto district (about 350 for the first time period and about 800 for the second period), calculate the differences between forward and backward runs (listed per year in Table 3) and estimate the average value for α per year. The data from 1884 are significantly less precise than the observations obtained in later years. Since this was the initial first order leveling campaign done in Japan, its lower precision is probably due to a different initial value for the field tolerance β. Because the leveling error remains relatively stable after the 1890s and the oldest data used in this study are from 1891, we exclude the 1884 α-value from our analysis. The lower row of Table 3 lists the formal values for $\tilde{\alpha}$, the average leveling error for each multiple year period, that we adopt here: 0.54 mm for the period before 1923 and 0.62 mm for the years 1923 to 1925. We smooth the leveling data for each route by removing obvious outliers and small-scale ($<$ 10km) deviations from the regional trend in the data. We utilize the tide gage record that shows a coseismic sea level change of 1.39 m at Aburatsubo (Figure 2) to establish an absolute reference frame for the elevation changes. The final leveling data set consists of 469 measurements (Table 2). Since leveling is a very precise technique for measuring surface deformation, its errors are very small compared to the errors of the angle

changes in triangulation surveys. This is illustrated by the difference in signal-to-noise ratio of both data types, which is 43.78 for the leveling data and 5.88 for the first and second order triangulation data combined (Table 2).

Figure 5 shows the vertical displacement data obtained along routes I through IX. The locations of strongest vertical deformation coincide with the areas of largest angle changes (section 2.1). The vertical coseismic deformation reveals uplifts of around 1.5 m on route I at the southern part of Boso Peninsula and on route II at the southernmost tip of Miura Peninsula. The maximum uplift of up to 2 m is measured along the coast at Odawara on route III. We omit from the final data set the part of route IV on Izu Peninsula that was measured immediately after the 1930 $M_s = 7.3$ Kita-Izu earthquake [*Matsuda,* 1972] (Figure 3). The region west of Tokyo along route V underwent subsidence with a maximum of 0.5 m. Towards the east in Tokyo and vicinity along routes VI and IX relatively small displacements, predominantly subsidence, were measured.

2.3. Postseismic and Interseismic Deformation

In this study we are most interested in the coseismic signal in the geodetic data set. Some of the individual measurements, however, span time intervals of several decades to a maximum of 40 years. With earthquake repeat times of 200 to 400 years for 1923-type events in the Sagami trough [*Shishikura*, 2003], these data time spans may account for 5 to 20% of the recurrence time. Assuming that the style and rate of deformation in the Kanto district are the same before and after the Kanto earthquake, some nominally coseismic observations must then be significantly influenced by interseismic deformation.

To adjust for these influences we integrate the interseismic velocity over the appropriate time interval at each site by using the interseismic model of *Nishimura and Sagiya* [2004] for the Kanto region based on continuous GPS data (Figure 6). The horizontal interseismic velocity field with respect to stable Eurasia is dominated by two effects: (1) the westward motion of the Pacific plate that is resisted by shallow locking along the Japan trench; and (2) the northwestward convergence of the Philippine Sea plate along the Sagami trough (Figure 6A). The southwestern part of Boso Peninsula, Miura Peninsula and the coastal area between Miura and Izu Peninsulas experience subsidence, while the rest of the area shows uplift (Figure 6B). Since the interseismic velocity field is opposite in sense to the coseismic deformation almost everywhere, adjustment of the coseismic data for interseismic deformation causes an overall increase in the coseismic signal. Adjustment for interseismic deformation has a stronger effect on the angle changes than on the leveling data, because on average the triangulation observations span longer time intervals and much of the leveling data is located farther from the interseismically most active region around the subduction zone. For angle changes the average adjustment is about 15% of the original observations, whereas for leveling data it is about 5%.

The postseismic geodetic surveys for both triangulation and leveling that are used in this study were done within 2 years after the 1923 event and postseismic afterslip and perhaps visco-elastic relaxation influence the records (see *Pollitz et al. [2004b]*). We have insufficient knowledge of its pattern and its magnitude to satisfactorily correct the coseismic signal in the geodetic data. However, available observations show that the postseismic deformation, accumulated between 1923 and 1925 is only a minor contaminant in the coseismic data and we make no corrections for postseismic effects.

3. Existing models

All existing models of the 1923 Kanto earthquake show right-lateral reverse slip and a fault plane location on the interface between the Philippine Sea plate and northern Honshu. However, some detailed features, listed in Table 4, show large variability. Figure 7 shows the projection onto the Earth's surface of fault planes of the studies discussed in this section. To quantitatively analyze the main characteristics of the existing models for the 1923 Kanto earthquake we compute misfits between the geodetic data used in this study and the predicted deformation for each model. To quantify the goodness of fit we use the normalized root-mean square (NRMS) misfit function, defined as

$$\mathrm{MF}_c = \sqrt{\frac{1}{N - dof} \sum_{n=1}^{N} \left(\frac{d_i - p_i}{(w_i \sigma_i)^2} \right)^2} \qquad (3)$$

with N the number of data, dof the number of degrees of freedom, d_i the ith observation, p_i the ith prediction, σ_i the standard deviation of d_i and w a weighting factor. Computation of the NRMS misfit for a data set consisting of both leveling and triangulation data would be dominated by the misfit between model and leveling data due to the high signal-to-noise ratio of the leveling data (Table 2). Introduction of w allows us to consider one data misfit value based on both leveling and triangulation data, without having the leveling data dominate the grid search in the modeling to be discussed in the next section. w_i is chosen as the ratio of the signal-to-noise ratios of leveling and triangulation data, with a value of 7.45 for leveling data (and 1.0 for triangulation data). To understand misfit values in terms of fit to both types of data we compute the misfit for triangulation (MF_T) and leveling (MF_L) data separately and for both data types combined (MF). Figure 8 and Table 4 display the three different misfit values for each of the models discussed next.

The first analysis of the 1923 earthquake mechanism by *Ando* [1971], based on triangulation data only, presented a uniform source model with right-lateral slip and a small reverse component on a low-angle fault plane in the Sagami trough. *Matsu'ura et al.* [1980] and *Matsu'ura and Iwasaki* [1983] inverted triangulation and leveling data for uniform source models with one and two planes. The variable slip model of *Wald and Somerville* [1995] is constrained by the leveling and triangulation data of *Matsu'ura et al.* [1980] and to a lesser extent by teleseismic records. Their fault plane, subdivided into 70 cells, is based on model II of *Matsu'ura et al.* [1980], but has a larger length and width so as to encompass the larger slipped area of the model by *Kanamori* [1971], which is based on seismic data. The distributed slip solution consists of two patches of large fault slip ($\approx$ 6 to 7 meters) on the plate interface that coincide with the location and size of the two rectangular dislocations of the two-plane uniform source model of *Matsu'ura* [1980]. The larger area with maximum slip is located at a depth of 10 km just southwest of the coast of Boso Peninsula and the smaller high slip patch is located at 15 km depth below Odawara. The three-fault model by *Pollitz et al.* [1996] consists of uniform slip sources and proposes an east-west trending active strike-slip fault in the southern tip of Boso, the Boso transform fault. The horizontal displacement data in this model have been adjusted for interseismic deformation. Although orientations for strike and rake vary strongly among the different models, the

majority of the models are in relatively close agreement on the orientation of the slip vector (Table 4).

Smaller misfits are found for the series of similar models by *Matsu'ura et al.* [1980] and *Matsu'ura and Iwasaki* [1983] (Figure 8, Table 4). The two-plane model of *Matsu'ura et al.* [1980] (Figure 7), fits the data well. As described in section 2.1, *Ando*'s [1971] relatively poor fit to the triangulation data is explained by *Matsu'ura et al.* [1980], who corrected for a reference frame error in the horizontal displacements derived from the triangulation data. Surprisingly, applying the additional degrees of freedom in the models by *Wald and Somerville* [1995] and *Pollitz et al.* [1996] does not result in a better data fit.

4. Uniform source models

4.1. Modeling results

Encouraged by the success of the simple earthquake models described in the previous section, we start our modeling procedure by fitting a single plane uniform slip source model to the geodetic data set. Following *Okada* [1985, 1992] this model describes the earthquake as a uniform dislocation on a rectangular fault plane with horizontal upper and lower boundaries in a isotropic, elastic uniform half-space. The dislocation is defined by 9 model parameters: longitude and latitude of a corner of the fault plane, length, width, strike, dip and depth of the upper edge of the fault plane, and magnitude and rake of the slip vector. The data misfit is computed with equation 3. In the initial modeling phase we make no additional a priori assumptions about the elastic dislocation source and we perform a systematic forward grid search over large ranges of the 9-dimensional parameter space to find the best-fitting source model. Guided by the parameter values that produce the best data fit, these ranges are narrowed down in subsequent grid searches to find a global minimum in the data misfit value MF_c. During the grid search we find that MF_c tends to slightly decrease with increasing depth of the upper edge of the fault plane (d in Figure 9A) up to a depth of about 10 km. However, the sensitivity of MF_c to d is very weak. Furthermore, the seismic data of *Noguchi* [2002] contour a Philippine Sea plate that is much shallower under Kanto. Therefore we constrain the maximum value of the search range of d to 5 km.

The minimum for MF_c resulting from the grid search is 7.0 for a model with a low-angle fault plane (dip is 27°) and right-lateral reverse slip of almost 6 m (Table 4, Figure 9A). The misfit values for the same model computed for each data type, MF_t for triangulation and MF_l for leveling, are 5.1 and 12.8, respectively. The solution closely resembles the solution by *Matsu'ura and Iwasaki* [1983], the principal differences being a larger slip and a somewhat deeper buried fault plane in our model.

Our final single-plane uniform source model fits the data better than any of the previously published models described in section 3 (Figure 8, Table 4). Despite the relatively good data fit, the results show a strong tradeoff between the triangulation data fit and the fit to the leveling data for several model parameters. Figure 10 shows the grid search results for the best fit to the triangulation (A) and leveling (B) data. Triangulation data tend to be fit best by a fault plane dipping at a very low angle ($\approx 20°$) with a length of ≈ 90 km, whereas leveling data favor a longer fault plane (≥ 110 km) with a steeper dip ($\approx 40°$) and a relative shift in location towards the southeast (of $\approx 0.2°$). Furthermore, slip based on triangulation data has a significantly larger strike-slip

component (rake $> 150°$) than slip predicted by leveling data alone (rake $= 134°$).

The dashed line in Figure 11 shows the predictions for the single plane model together with the measurements of vertical deformation for the leveling routes, indicated by the colored lines. Only where the vertical interseismic displacements have a visible deviation from zero are they plotted. The modeled uplift on Boso Peninsula along route I is too large by about half a meter, while the model underestimates the uplift near Odawara along route III. The predicted subsidence along route V, in the area west of Tokyo, is larger than what is measured. The remaining main characteristics of the leveling data are fit by our optimal single plane source model. The largest misfits of the angle change data are located in the areas where the largest horizontal deformation is measured; on the southern part of Boso Peninsula, on Miura Peninsula and along the Odawara coastline. Figures 12A and B show that this simple model fits the first order triangulation data well, while it generally underestimates the second order angle changes.

In the next modeling phase we introduce a second fault plane. To reduce the number of model parameters we make some a priori assumptions based on the results for a single plane model (hereinafter model 1). The location and width of the eastern edge of the first plane are adopted from model 1. The location of the second fault plane is west of the first plane and the planes are connected at the top. Furthermore, for both planes we assume the same dip and buried depth prescribed by model 1. The remaining 9 model parameters to be solved for in this new series of grid searches are: strikes and lengths of both fault planes, width of the second fault plane and orientation and magnitude of slip on both planes.

The results for the optimal two-plane uniform source model (hereinafter model 2) are listed in Table 4. The two plane model has 14 degrees of freedom, 5 more than the single plane model. The combined data misfit value MF_c is 6.3 for model 2 (Figure 9B). The misfit value for triangulation data, $MF_t = 5.1$, has not changed with respect to the single plane model. However, the fit to the leveling observations, $MF_l = 8.8$, has significantly improved. Application of an F-test shows that the improvement of the fit of the combined data set with respect to the single plane model is significant. Although the trade-off between triangulation and leveling data is still present for some model parameters, the ranges over which the model parameters for MF_t and MF_l vary are reduced considerably. Only the magnitude of slip on the 2 planes show relatively large variations of approximately 1 to 1.5 m. Unlike the single plane model, the two plane model fits the uplift near Odawara along route III and the subsidence along route V, while it still overestimates uplift on Boso Peninsula along route I by approximately 0.5 meter(see Figure 11). Since this two fault plane model fits the main characteristics of the triangulation and leveling data, we adopt it as our preferred static source model for the 1923 earthquake.

4.2. Influence of a layered Earth

We investigate to what extent the predicted deformation field of solution 2 in a uniform half-space model differs from that in a more realistic, layered Earth model. We apply the method of *Wang* [1999] and *Wang et al.* [2003] to calculate static coseismic deformation in an isotropic, elastic continuum which consists of an arbitrary but finite number of laterally homogeneous layers, with the deepest layer extending to infinite depth. To represent the crust below Tokyo we use the layered velocity

structure obtained by *Takeo and Kanamori* [1992, 1998], listed in Table 5. This structure is derived from a combination of reflection, refraction, borehole and seismic data obtained in the Kanto region.

We compute horizontal and vertical surface deformation with the preferred 2 plane model in a layered crust and compare the results with those of the uniform half-space model. Overall, we find that the influence of layering is minor and most noticeable in those areas where the strongest coseismic deformation was measured; Boso and Miura Peninsula and Odawara (Figure 13).

Tokyo is located on the Kanto plain, which is covered by soft sedimentary layers with a total thickness of about a kilometer (upper layer in Table 5). These sediments are absent at the southern tips of Boso and Miura Peninsulas, and at western Kanto and Izu Peninsula [*Sato et al.*, 1998a]. The inclusion of this thin upper layer in ground motion modeling is significant [*Takeo and Kanamori*, 1992, 1997; *Sato et al.*, 1998a, 1998b]. However, it does not influence the static deformation field, since we find no significant differences between deformation computed with and without this top layer.

In addition, we tested two additional layered velocity structure models for Kanto, proposed in independent studies by *Yamazaki et al.* [1992] and *Sato* [1998a, 1998b], with and without soft, sedimentary layers on top. We find that all produce results similar to those obtained using the velocity structure of *Takeo and Kanamori* [1992].

5. Summary and discussion

We use an unprecedented dense historical geodetic data set consisting of triangulation and leveling data that is adjusted for interseismic deformation to model the source mechanism of the 1923 Kanto earthquake in terms of an elastic dislocation. The model that optimally fits the data consists of two adjacent low-angle planes accommodating uniform, reverse dextral slip of 7.4 m and 6.6 m with azimuths of 145° and 160°, respectively. Since the data fit is not sensitive to the application of a layered velocity structure, the preferred source model is defined in a uniform half-space.

5.1. Data fit

Although our preferred model fits the data better than any of the previously proposed models, the normalized misfit remains above 5 (Figure 8), whereas a real fit would give about 1.

For the leveling data the large normalized misfit is partly due to the small data standard deviations. Our model only fits the first-order characteristics of the vertical displacement data. The largest higher-order variations in the vertical displacement field are of the order of centimeters per km (for example Figure 11I), whereas the average formal data error is of the order of millimeters per km (Table 3). Furthermore, systematic errors can cause the elevation measurements to drift systematically along the leveling line leading to large data misfits.

For the triangulation data the large normalized misfit is mainly due to the fit of the second order triangulation data (Figure 12a and b): The trend in Figure 12b differs significantly from one. One possible explanation is the uneven distribution of the first- and second order triangulation data over the model area. Figure 2 shows that the first order data hardly record the deformation of the Boso Peninsula, whereas the second order data densely cover this region. The large misfit for the second order data may suggest that our model needs more complexity to correctly represent the coseismic deformation

on Boso Peninsula. Furthermore, since the second order data cover on average longer time intervals than the first order data, an incorrect interseismic deformation rate will produce a larger misfit for the second order data.

5.2. Location of the fault plane

The fault planes and isodepth contours of our preferred source model are plotted in Figure 14 together with the isodepth contours of the Philippine Sea plate by *Noguchi* [2002]. Our model is very similar to model III of *Matsu'ura et al.* [1980] (see Figure 1C). Although the projections of the two models onto the Earth's surface almost completely overlap, our fault planes are located 1.5 km deeper and the width of the western plane is much longer and penetrates deeper into the Earth. In general, our smaller fault plane and the western rim of our larger fault plane fit the isodepth contours of the Philippine Sea plate well. Due to lack of resolution *Noguchi* [2002] did not interpret the isodepth contours of the Philippine Sea plate at the location of our eastern fault plane. The locations of the centers of our two planes coincide with the locations of the two patches of high 1923 coseismic slip in the source model of *Wald and Somerville* [1995].

According to *Kanamori and Miyamura* [1970], who interpreted seismic observations, the 1923 earthquake nucleated beneath the Odawara region at latitude 35.4°, longitude 139.2° at a depth between 10 and 15 km (star in Figure 14), which coincides with the location of the western fault plane.

A recent seismic reflection study of Sagami Bay and surrounding coastal areas by *Sato et al.* [2003] revealed what may be the continental continuation of the northwestern segment of the interplate thrust fault: a narrow, concentrated zone (< 1 km) of reflectors. A 40-km long seismic section shows this zone of east dipping reflectors at a depth of about 4 km beneath Odawara (white circle in Figure 14) and at Kamakura (at the northern end of Miura Peninsula) at a depth of about 13 km (black circle in Figure 14). In addition, the seismic data suggest that the northeastward dipping Kozu-Matsuda fault (m in Figure 14) and northward dipping Kannawa thrust fault (k) [*Ando,* 1974; *Niitsuma*, 1999] are on-land splay-faults of the continental continuation of the plate interface. The seismic study of *Sato et al.* [2003] shows that the deeper extension of the Kozu-Matsuda fault merges into a narrow zone of east dipping reflectors at about 6.5 km in depth beneath the Oiso hills (white square in Figure 14). The locations of these reflectors coincide with the locations of the planes of our source model.

5.3. Slip orientation

Azimuths of the coseismic slip vectors in our source model are 160° for the eastern plane and 145° for the western plane (Table 4). They are oriented more normal to the strike of the fault plane than are the relative plate motion vectors (Figure 15). This suggests that along the larger eastern plane, relative plate motion is partitioned and part of the boundary-parallel plate motion is taken up elsewhere. The orientation of the western plane with respect to the direction of relative plate motion allows it to accommodate the convergence more efficiently than the eastern plane.

As a possible candidate for accommodating the plate-parallel motion, *Lallemant et al.* [1996] and *Pollitz et al.* [1996] propose the Boso Transform fault. According to these authors, this fault is a right-lateral strike-slip fault that surfaces at the southern tips of Boso and Miura Peninsulas. They further propose that it ruptured dur-

ing the 1923 Kanto earthquake. The surface fault traces are indicated by *b*'s in Figure 14. However, the coseismic triangulation and present-day continuous GPS data do not indicate any significant dextral surface deformation across these fault segments and in other studies these faults are considered to be splay-faults from the subduction plate interface [e.g., *Saito et al.,* 2002]. Therefore, if slip partitioning occurs to make up for the mismatch between the 1923 earthquake slip vector and the expected interplate convergence direction, it is uncertain whether the proposed Boso transform can accommodate the expected right-lateral strike-slip motion.

5.4. Slip magnitude

We compare our 1923 coseismic slip with relative plate motion predicted by plate tectonic models and with a recurrence model derived from uplift records of marine terraces. Subduction of the Pacific plate along the Japan and Izu-Bonin trenches accommodates convergence between the Pacific, northern Honshu and the Philippine Sea plates. The velocity of the Pacific plate with respect to northern Honshu at the latitude of the Sagami trough is about 75 mm/yr in a westward direction [*Seno et al.*, 1996]. The Philippine Sea plate subducts beneath Honshu along the Nankai, Suruga and Sagami troughs. The existing plate motion models predict between 30 mm/yr at an azimuth of 142° [*Sella et al.* 2002] based on GPS data, 29 mm/yr at an azimuth of 143° [*Seno et al.* 1993, 1996] based on earthquake slip vectors, and 45 mm/yr at an azimuth of 133° [*Heki et al.* 1999; *Miyazaki and Heki* 2001] based on GPS data. For all models, the convergence between the Philippine Sea plate and northern Honshu at the Sagami Trough is highly oblique (Figure 16).

There is a 220 year time interval between the 1923 Kanto earthquake and the last big event that ruptured the same plane, the 1703 Genroku M_s=8.1 event. Assuming that 100% of the relative plate motion is released by major earthquakes in the Sagami trough, 220 years of accumulating plate motion would result in coseismic slip of 6.6 m at an azimuth of 142° according to *Sella et al.* [2002], 8.6 m at an azimuth of 143° for the model of [*Seno et al.,* 1993, 1996] and 9.9 m at an azimuth of 133° following *Heki et al.* [1999] and *Miyazaki and Heki* [2001]. While the slip estimates according to the plate models of *Seno* [1993, 1996] and *Sella* [2002] are in acceptable agreement with the slip predicted by our model on the larger of the two fault planes, the third model predicts coseismic slip that is 20 to 30% larger than our modeling results.

Uplift records of marine terraces along Boso and Miura Peninsula show a regular pattern of earthquake activity over the past 7,250 years and seem to indicate that two different types of megathrust earthquakes occur on the Sagami Trough [*Matsuda et al.*, 1978; *Shishikura*, 2003]. A smaller type of event associated with the 1923 Kanto earthquake causes average uplifts of 1.2 to 1.5 meters every 400 years (± 200 years), while a larger type of event, associated with the M_s=8.1 earthquake that hit Kanto in 1703, causes average uplifts of 3 meters every 2300 years (± 800 years). The vertical displacement caused by the former type of event agrees with our model results. The latter type of event is assumed to rupture over a larger area, extending eastwards from the fault plane derived for the 1923 Kanto earthquake [*Shishikura et al.,* 2005].

Assuming 100% seismic release, convergence rates of 30-45 mm/yr measured by GPS, accumulated over the average recurrence times of 400 years suggested by the marine terrace uplift record, would result in average,

characteristic events for the Sagami trough with horizontal coseismic displacements of 12 to 18 m. These slip values require earthquakes that are much larger than the 1923 earthquake. Furthermore, they contradict the moderate height of about 1.2 to 1.5 m of the terraces associated with this 400 year time interval, which can be fit by a 1923-type event (and is predicted by our model).

In summary, several important questions pertaining to the seismic hazard in the Tokyo Bay area remain to be solved. Seismic hazard in the Tokyo Bay area can not be assessed by a simple recurrence model with characteristic earthquakes. Although the 1923 coseismic slip magnitude can be explained by plate motion models of *Seno et al.* [1993, 1996] and *Sella et al.* [2002], the marine terrace record combined with this study's results suggest an alternative mechanism or a combination of mechanisms is responsible for accommodating a slip deficit of up to 50% of the total plate motion across the Sagami trough per average recurrence time interval of 400 years.

Several recent studies propose mechanisms that may resolve some of the problems. The M_s=7.2 1855 Ansei Edo earthquake caused severe damage to Tokyo. Most studies agree on its epicenter being located near Tokyo, while its focal depth and mechanism are debated. Estimated sources include a shallow crustal event, an interplate event on the Philippine Sea Plate-Honshu interface and an intraplate event in the Pacific plate [*Bakun*, 2004 *and references therein*]. Newly interpreted intensity data from the catalogue of *Usami* [1996] best fit a location on either the lower extension of the Philippine Sea plate, the Philippine Sea-Pacific plate interface or the top of the Pacific plate [*Bakun*, 2004]. Based on the abundance of aftershocks recorded of the 1855 earthquake, *Bakun* [2004] locates the event on the lower extension of the Philippine Sea plate at a depth of 30 km, just below the part that ruptured during the 1923 earthquake. If this type of event occurs on a regular basis, it may account for a small part of the accommodation of plate motion, since one can expect the rupture to propagate upwards and release some of the accumulated slip deficit on the plate interface between the surface and 30 km. Unfortunately, the historic earthquake record does not allow for a systematic recognition of Ansei Edo-type events before 1855.

A more promising direction of future research may be the discovery of silent slip events. *Ozawa et al.* [2003] discovered the signal of slow earthquakes on a part of the downgoing slab of the Philippine Sea plate that is located in the Sagami trough southeast of the southern tip of Boso Peninsula. Two silent slip events with an interevent time of 6 years and slip of up to 20 cm were detected. If events like this occur on a regular basis they can account for most or all of the accumulated plate motion predicted by the models of *Sella et al.* [2002], *Seno et al.* [1993, 1996]) and *Heki et al.* [1999]. However, these slip events occurred east of the segments that ruptured during the 1923 event, on which, so far, no evidence has been found for silent slip.

Acknowledgments. We would like to thank Bill Bakun, Tom Parsons, Ross Stein and Shinji Toda for extremely useful discussions during various stages of this research. Thorough reviews by Jim Savage and Jessica Murray improved this manuscript considerably. We are grateful to Masanobu Shishikura for organizing a field trip to Boso Peninsula and for explaining his work on the dating of the uplift of marine terraces. We acknowledge the help of Mitsuo Ohtaki from GSI in Tsukuba, who computed the errors in the leveling measurements obtained after 1955. Most of the figures in this paper were produced using the public domain GMT software package [*Wessel and Smith*, 1995].

References

Ando, M., A fault-origin model of the Great Kanto earthquake of 1923 as deduced from geodetic data, *Bulletin of the Earthquake Research Institute, 49*, 19–32, 1971.

Ando, M., Seismo-tectonics of the 1923 Kanto earthquake, *J. Phys. Earth, 22*, 263–277, 1974.

Bakun, W. H., Magnitude and location of historical earthquakes in Japan and implications for the 1855 Ansei Edo earthquake, *submitted to J. Geophys. Res.*, 2004.

Bibby, H. M., Unbiased estimate of strain from triangulation data using the method of simultaneous reduction, *Tectonophysics, 82*, 161–174, 1982.

Bomford, G., *Geodesy,* 855 pp., Clarendon, Oxford, 1980.

Frank, F. C., Deduction of earth strains from survey data, *Bull. Seismol. Soc. Am., 56*, 35–42, 1966.

Fujii, Y., and K. Nakane, Horizontal crustal movements in the Kanto-Tokai district, Japan, as deduced from geodetic data, *Tectonophys., 97*, 115–140, 1983.

Harris, R., Introduction to special section: Stress triggers, stress shadows, and implications for seismic hazard, *J. Geophys. Res., 95,* 24,347–24,358, 1998.

Heki, K., S. Miyazaki, H. Takahashi, M. Kasahara, F. Kimata, S. Miura, N. Vasilenko, A. Ivaschenko, and K.-D. An, The Amurian Plate motion and current plate kinematics in eastern Asia, *J. Geophys. Res., 104,* 29,147–29,155, 1999.

Huchon, P., and H. Kitazato, Collision of the Izu block with central Japan during the Quaternary and geological evolution of the Ashigara area, *Tectonophysics, 110,* 201–210, 1984.

Ishibashi, K., Specification of a soon-to-occur seismic faulting in the Tokai district, central Japan, based upon seismotectonics, in *Earthquake Prediction; an International Review,* edited by D. Simpson and P. Richard, pp. 297–332, AGU, Washington, D.C., 1981.

Ishibashi, K., Kanagawaken-Seibu-Earthquake and earthquake prediction I (*in Japanese*), *Kagaku, 58*, 537–547, 1988.

Ishida, M., Geometry and relative motion of the Philippine Sea Plate and Pacific plate beneath the Kanto-Tokai district, Japan, *J. Geophys. Res., 97*, 489–513, 1992.

Ishida, M., and M. Kikuchi, A possible foreshock of a future large earthquake near Odawara, center Japan, *Geophys. Res. Lett., 19*, 1695–1698, 1992.

Japan Association of Surveyors, History of surveying and mapping for one hundred years *in Japanese*, edited by Editorial Committee for History of Surveying and Mapping for one hundred years, 673 pp., Japan Association of Surveyors, Tokyo, 1970.

Kanamori, H., Faulting of the Great Kanto earthquake of 1923 as revealed by seismological data, *Bull. Earthq. Res. Inst., 49*, 13–18, 1971.

Kanamori, H., and S. Miyamura, Seismometrical re-evaluation of the Great Kanto earthquake of September 1, 1923, *Bull. Earthq. Res. Inst., 48*, 115–125, 1970.

Lallemant, S. J., X. Le Pichon, F. Thoue, P. Henry, and S. Saito, Shear partitioning near the central Japan triple junction: the 1923 great Kanto earthquake revisited - I, *Geophys. J. Int., 126*, 871–881, 1996.

Marshall, G. A., R. S. Stein, and W. Thatcher, Faulting geometry and slip from co-seismic elevation changes: The 18 October 1989, Loma Prieta, California, earthquake, *Bull. Seismol. Soc. Am., 81*, 1660–1693, 1991.

Matsuda, T., Surface faults associated with the Kita-Izu earthquake of 1930 in Izu Peninsula, Japan, in *The Izu Peninsula,* edited by M. Oshino and H. Aoki, pp. 77–93, Tokai Univ. Press, Tokyo, 1972.

Matsuda, T., Y. Ota, M. Ando, and N. Yonekura, Fault mechanism and recurrence time of major earthquakes in Southern Kanto district, Japan, as deduced from coastal terrace data, *Geol. Soc. Amer. Bull., 89,* 1610–1628, 1978.

Matsu'ura, M., T. Iwasaki, Y. Suzuki, and R. Sato, Statical and dynamical study on faulting mechanism of the 1923 Kanto earthquake, *J. Phys. Earth, 28*, 119–143, 1980.

Matsu'ura, M., and T. Iwasaki, Study on coseismic and postseismic crustal movements associated with the 1923 Kanto earthquake, *Tectonophys, 97*, 201–215, 1983.

Military Land Survey, Re-survey of the Kwanto district after the great earthquake of 1923, *Bull. Imp. Earthq. Invest. Comm., 11*, 1–6, 1930.

Miyabe, N., On the vertical movement in Kwanto districts, *Bull. Earthq. Res. Inst., Univ. Tokyo, 9,* 1–21, 1931.

Miyazaki, S., and K. Heki, Crustal velocity field of Southwest Japan: Subduction and arc-arc collision, *J. Geophys. Res., 106,* 4305–4326, 10.1029/2000JB900312, 2001.

Muto, K., A study of the displacements of triangulation points, *Bull. Earthq. Res. Inst., Univ. Tokyo, 10,* 384–392, 1932.

Niitsuma, N., Rupture and delamination of island arc crust due to the arc-arc collision in the South Fossa Magna, central Japan, *The Island Arc, 8*, 441–458, 1999.

Nishimura, T., and T. Sagiya, Crustal block kinematics around the northern Philippine Sea plate, central Japan, estimated from GPS and leveling data, *in preparation*, 2005.

Noguchi, S., Earthquake clusters in the Kanto and Tokai subduction zones: Implications for modes of plate consumption, in *Seismotectonics in Convergent Plate Boundary,* edited by Y. Fujinawa and A. Yoshida, pp. 451–467, TERRAPUB, Tokyo, 2002.

Nyst, M., N. Hamada, F.F. Pollitz, and W. Thatcher, The stress triggering role of the 1923 Great Kanto earthquake, *to be submitted to J. Geophys. Res.*, 2005.

Ohtake, M., A unified seismotectonic model for Kanto and Tokai regions: mechanics of shallow south Kanto earthquakes *in Japanese*, *Bosai-Kagaku-Gijyutsu, (NIED report), 41,* 1–7, 1980.

Okada, Y., Surface deformation due to shear and tensile faults in a half space, *Bull. Seismol. Soc. Am., 75*, 1135–1154, 1985.

Okada, Y., Internal deformation due to shear and tensile faults in a half-space, *Bull. Seis. Soc. Am., 82*, 1018–1040, 1992.

Ozawa, S., S. Miyazaki, Y. Hatanaka, T. Imakiire, M. Kaidzu, M. Murakami, Characteristic silent earthquakes in the eastern part of the Boso peninsula, Central Japan S. Ozawa, *Geophys. Res. Lett., 30*, 1283, 10.1029/2002GL016665, 2003.

Pollitz, F. F., X. Le Pichon and S. J. Lallemant, Shear partitioning near the central Japan triple junction: the 1923 great Kanto earthquake revisited - II, *Geophys. J. Int., 126*, 882–892, 1996.

Pollitz, F. F., M. Nyst, and W. Thatcher, Coseismic slip distribution of the 1923 Kanto earthquake, Part II, *to be submitted to J. Geophys. Res.,* 2005a.

Pollitz, F. F., M. Nyst, and W. Thatcher, Inference of postseismic deformation mechanisms following the 1923 Kanto earthquake, *to be submitted to J. Geophys. Res.,* 2005b.

Sagiya, T., and W. Thatcher, Coseismic slip resolution along a plate boundary megathrust: The Nankai Through, southwest Japan, *J. Geophys. Res., 104*, 1111–1129, 1999.

Sagiya, T., S. Myazaki and T. Tada, Continuous GPS array and present-day crustal deformation of Japan, *Pure Appl. Geophys., 157*, 2303–2322, 2000.

Saito, T., and M. Ito, Deposition of sheet-like turbidite packets and migration of channel-overbank systems on a sandy submarine fan: an example from the Late Miocene-Early Pliocene forearc basin, Boso Peninsula, Japan , *Sedimetary Geology, 149*, 265–277, 2002.

Sato, T., D. V. Helmberger, P. G. Somerville, R. W. Graves and C. K. Saikia, Estimates of regional and local strong motions during the Great 1923 Kanto, Japan, Earthquake (*Ms* 8.2). Part 1: Source estimation of a calibration event and modeling of wave propagation paths, *Bull. Seismol. Soc. Am., 88,* 183–205, 1998a.

Sato, T., R. W. Graves, P. G. Somerville, and S. Kataoka, Estimates of regional and local strong motions during the Great 1923 Kanto, Japan, earthquake (*Ms* 8.2). Part 2: Forward simulation of seismograms using variable-slip rupture models and estimation of near-fault long-period ground motions, *Bull. Seismol. Soc. Am., 88,* 206–227, 1998b.

Sato, H., and 11 others, Deep seismic reflection profiling in the source region of the 1923 Kanto Earthquake, *Eos. Trans. AGU, 84(46)*, Fall Meet. Suppl., Abstract S51G-01, 2003.

Savage, J. C., and R. O. Burford, Accumulation of tectonic strain in California, *Bull. Seismol. Soc. Am., 60*, 1877–1896, 1970.

Sella, G. F., T. H. Dixon, and A. Mao, REVEL: A model for Recent plate velocities from space geodesy, *J. Gephys. Res., 107,* 10.1029/2000JB000033, 2002.

Seno, T., S. Stein, and A. E. Gripp, A model for the motion of the Philippine Sea plate consistent with NUVEL-1 and geological data, *J. Geophys. Res., 98,* 17941–17948, 1993.

Seno, T., T. Sakura, and S. Stein, Can the Okhotsk plate be discriminated form the North American plate? *J. Geophys. Res., 101,* 11,305–11,315, 1996.

Shishikura, M., Cycle of Interplate Earthquake Along the Sagam Trough, Deduced from Tectonic Geomorphology, *Bull. Earthq. Res. Inst. Univ. Tokyo, 78,* 245–254, 2003.

Shishikura, M., S. Toda, and K. Satake, Fault model of the 1703 Genroku Kanto Earthquake (M=8.2) along the Sagami Trough deduced from renewed coseismic crustal deformation, *in preparation*, 2005.

Takeo, M., and H. Kanamori, Simulation of long-period ground motions for the 1923 Kanto earthquake (M = 8), *Bull. Earthquake Res. Inst. Tokyo Univ., 67,* 389–436, 1992.

Takeo, M., and H. Kanamori, Simulation of Long-Period Ground Motion near a Large Earthquake, *Bull. Seismol. Soc. Am., 87,* 140–156, 1997.

Thatcher, W., Strain accumulation and release mechanism of the 1906 earthquake, *J. Geophys. Res., 80*, 4862–4872, 1975.

Thatcher, W., Order and diversity in the modes of circum-Pacific earthquake recurrence, *J. Geophys. Res., 95,* 2609–2623, 1990.

Toda, S., R. S. Stein, P. A. Reasenberg, J. H. Dieterich, and A. Yoshida, Stress transferred by the 1995 $M_w = 6.9$ Kobe, Japan, shock: Effects on aftershocks and future earthquake probabilities, *J. Geophys. Res., 95,* 24,543–24,566, 1998.

Tsukahara, H., and R. Ikeda, Hydraulic fracturing stress measurements and in-situ stress field in the Kanto-Tokai area, Japan, *Tectonophysics, 135,* 329–345, 1987.

Usami, T., Materials for comprehensive list of destructive earthquake in Japan (*in Japanese*), *Univ. of Tokyo Press*, 1996.

Walcott, R. I., The kinematics of the plate boundary zone through New Zealand: A comparison of short and longterm deformations, *Geophys. J. R. Astron. Soc., 79*, 613–633, 1984.

Wald, D. J., and P. G. Somerville, Variable-slip rupture model of the great 1923 Kanto, Japan, earthquake: Geodetic and body-waveform analysis, *Bull. seismol. Soc. Am., 85*, 159–177, 1995.

Wang, R., A simple orthonormalization method for the stable and efficient computation of Green's functions, Bull. Seism. Soc. Am., 89, 733–741, 1999.

Wang, R., F. Lorenzo, and F. Roth, Computation of deformation induced by earthquakes in a multi-layered elastic crust – FORTRAN programs EDGRN/EDCMP, *Computers and Geosciences, 29*, 195–207, 2003.

Wessel, P., and W. H. F. Smith, New, improved version of the Generic Mapping Tools Released, *EOS Trans. AGU, 79,*, 579, 1998.

Yamanaka, H., Analysis and modeling of long-period ground motion in the Kanto plain, Japan, *Proc. of the 4th International Conference Seismic Zonation,* 75–82, 1991.

Yamazaki, K., M. Minamishima, and K. Kudo, Propagation characteristics of intermediate-period (1-10seconds) surface waves in the Kanto Plain, Japan, *J. Phys. Earth, 40,* 117–136, 1992.

Yu, E., and P. Segall, Slip in the 1868 Hayward earthquake from the analysis of historical triangulation data, *J. Geophys. Res., 101,* 16,101–16,118, 1996.

M. Nyst, Department of Geophysics, Stanford University, Stanford, USA. (mnyst@pangea.stanford.edu)

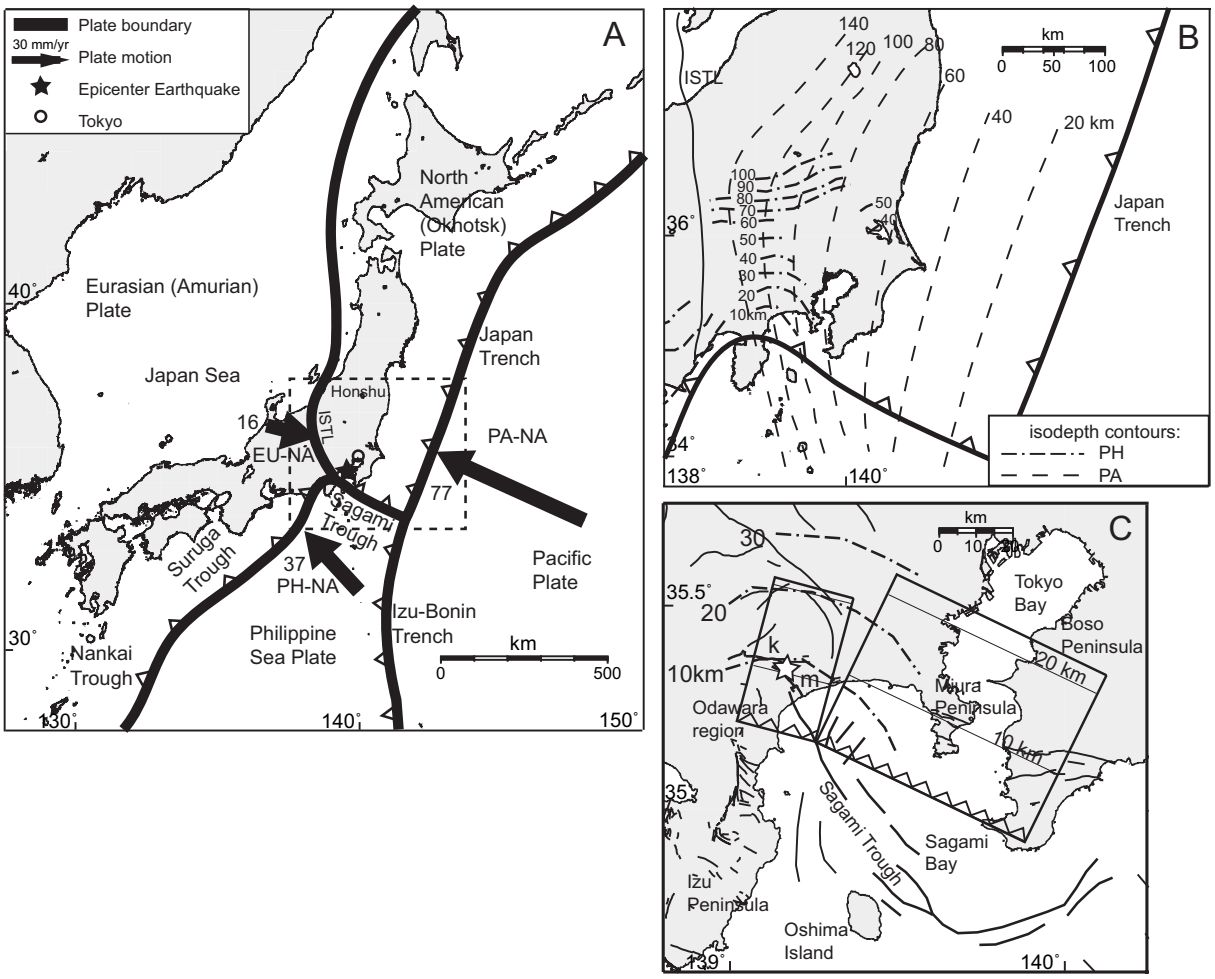

Figure 1. (A) Plate tectonic setting of Japan, where four major plates converge: the Eurasian (EU) or Amurian according to *Heki et al.* [1999]; *Miyazaki and Heki* [2001] and *Sella et al.* [2002], North American (NA) or Okhotsk according to *Seno et al.* [1993, 1996] and *Sella et al.* [2002], Pacific (PA) and Philippine Sea (PH) plate. Northern Honshu is located on the North American or Okhotsk plate. ISTL Itoigawa-Shizuoka Tectonic Line. The arrows indicate motion of different plates relative to northern Honshu, the numbers are averages of the rate predictions in mm/yr, based on Global Positioning System (GPS) observations [*Heki et al.* 1999, *Seno et al.* 1996]. The dashed square outlines the area shown in (B); (B) Isodepth contours of the surfaces of the PH and the PA plates based on seismicity data and the contact zone between the two plates [from *Noguchi*, 2002]; (C) Active fault map of the coastal region around Sagami Bay with 1923 coseismic fault model planes (III) of *Matsu'ura et al.* [1980] and isodepth contours of the Philippine Sea plate [*Noguchi*, 2002]. The star indicates the epicenter of the 1923 Kanto earthquake according to the seismic study of *Kanamori and Miyamura* [1970]. Bold printed lines indicate the Sagami Trough, NNW-SSE striking Kozu-Matsuda (indicated by m) and E-W striking Kannawa (indicated by k) fault systems.

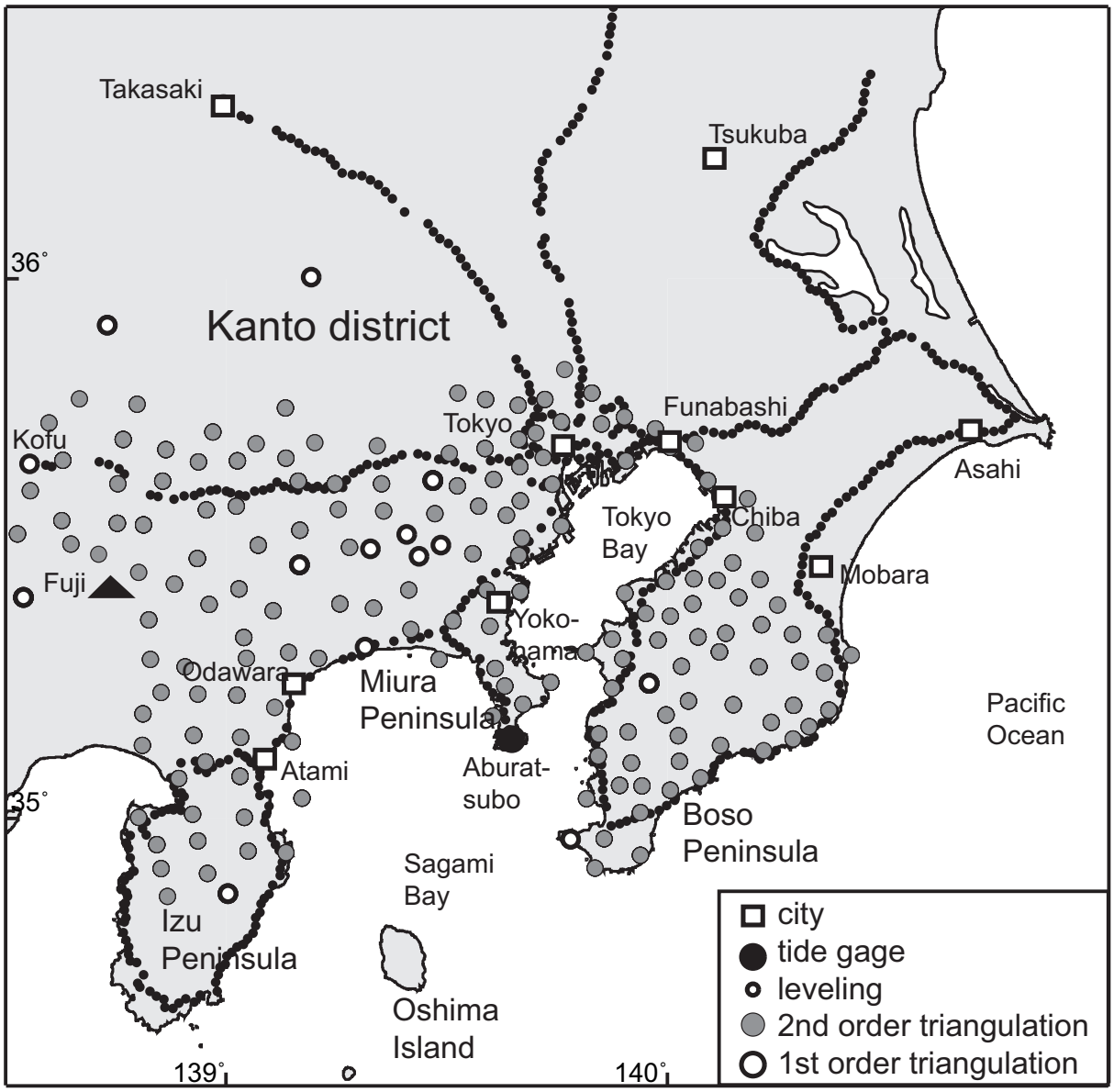

Figure 2. The geodetic observation networks used in this study. The leveling data are tied to an absolute vertical reference frame by using the tide gage records of Aburatsubo station.

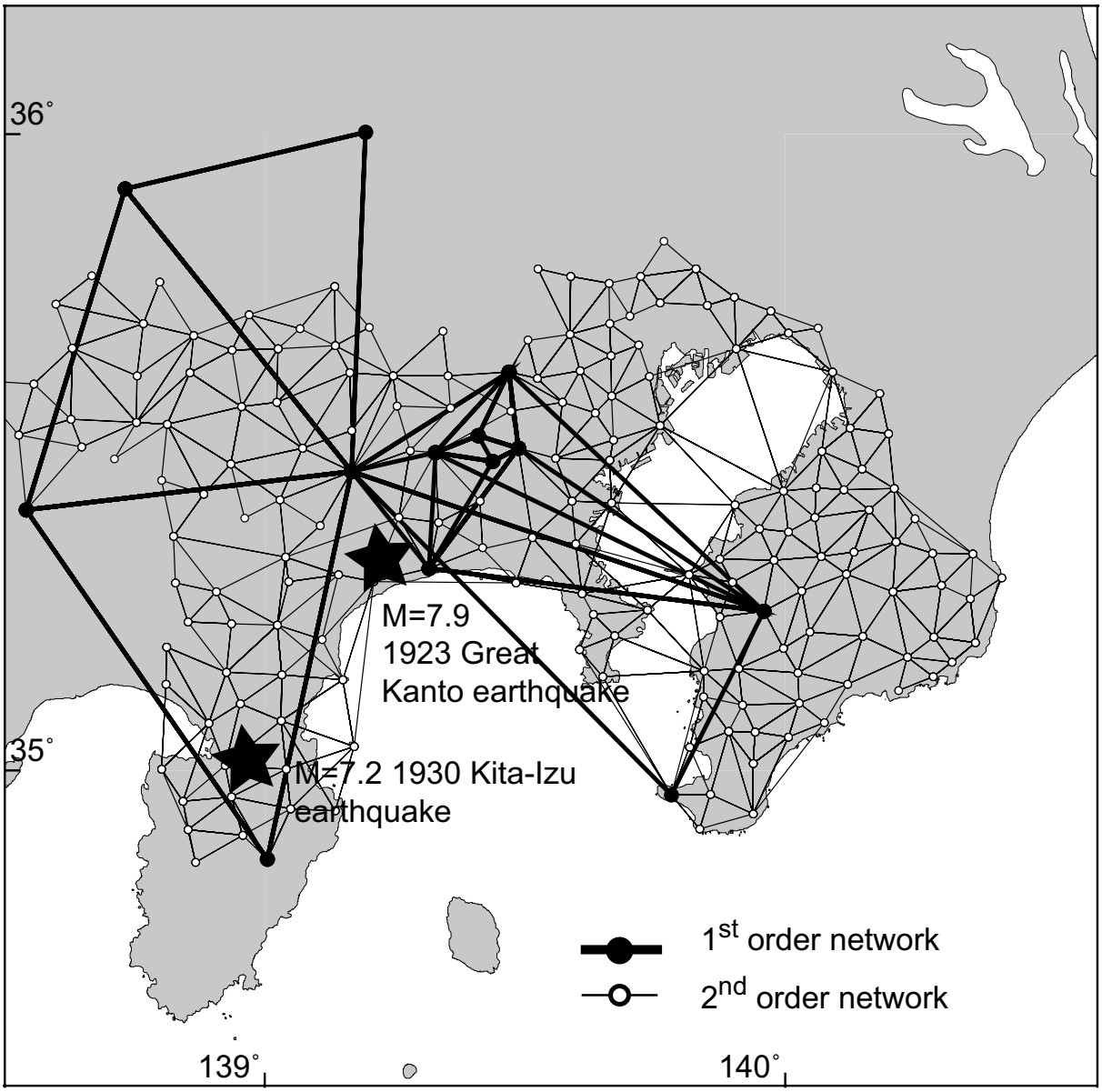

Figure 3. First and second order triangulation networks where repeated angles are available. Stations without repeated angle observations do not contribute to the data set used in this study and are not shown here.

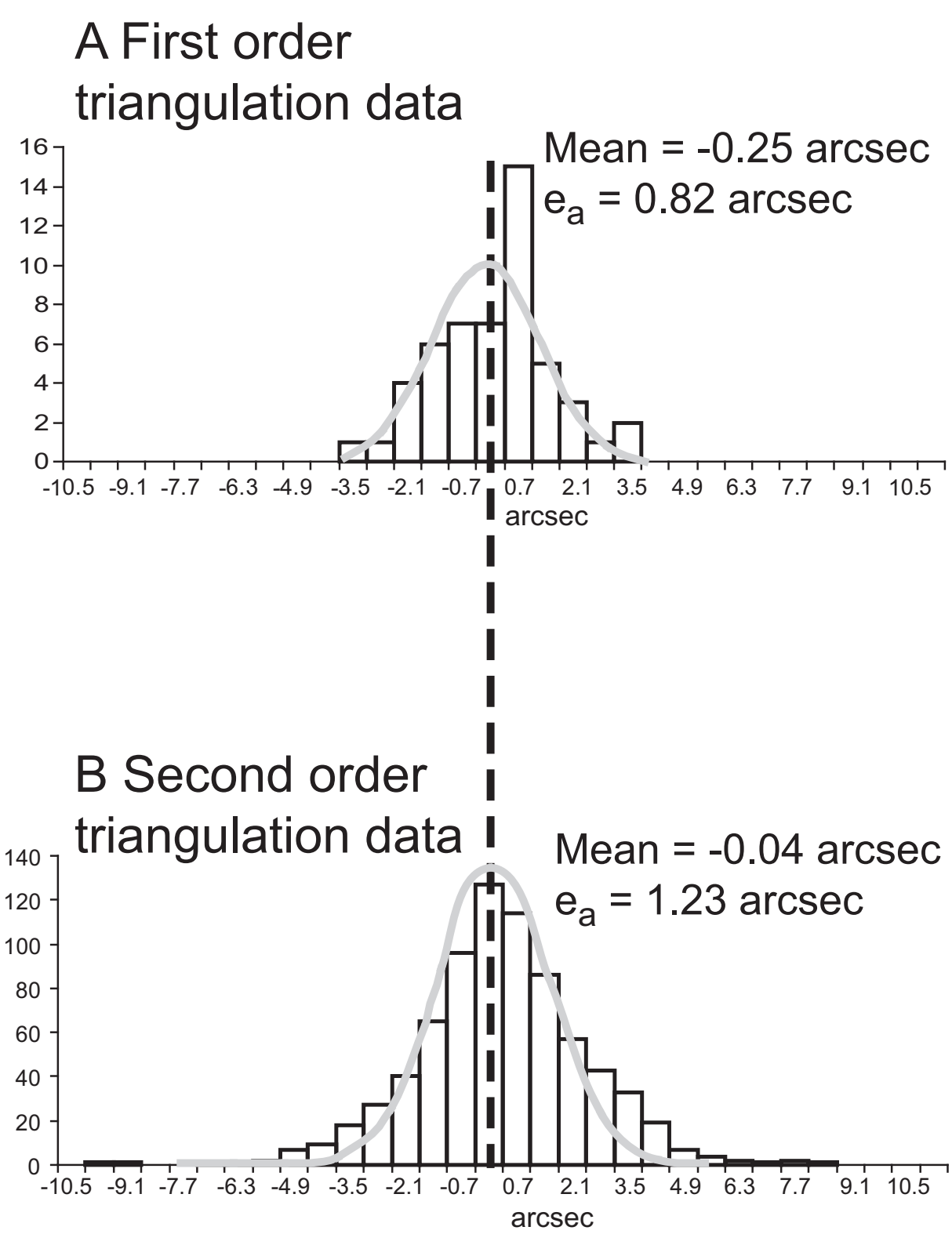

Figure 4. Results of the error analysis of the triangulation data (see also Table 1). Solid line shows Gaussian curve fit to the data. (A) Frequency distribution of the first order triangle closures (equation 1). ϵ_a indicates the average observational error computed with equation 2; (B) Same as (A) for second order triangulation data.

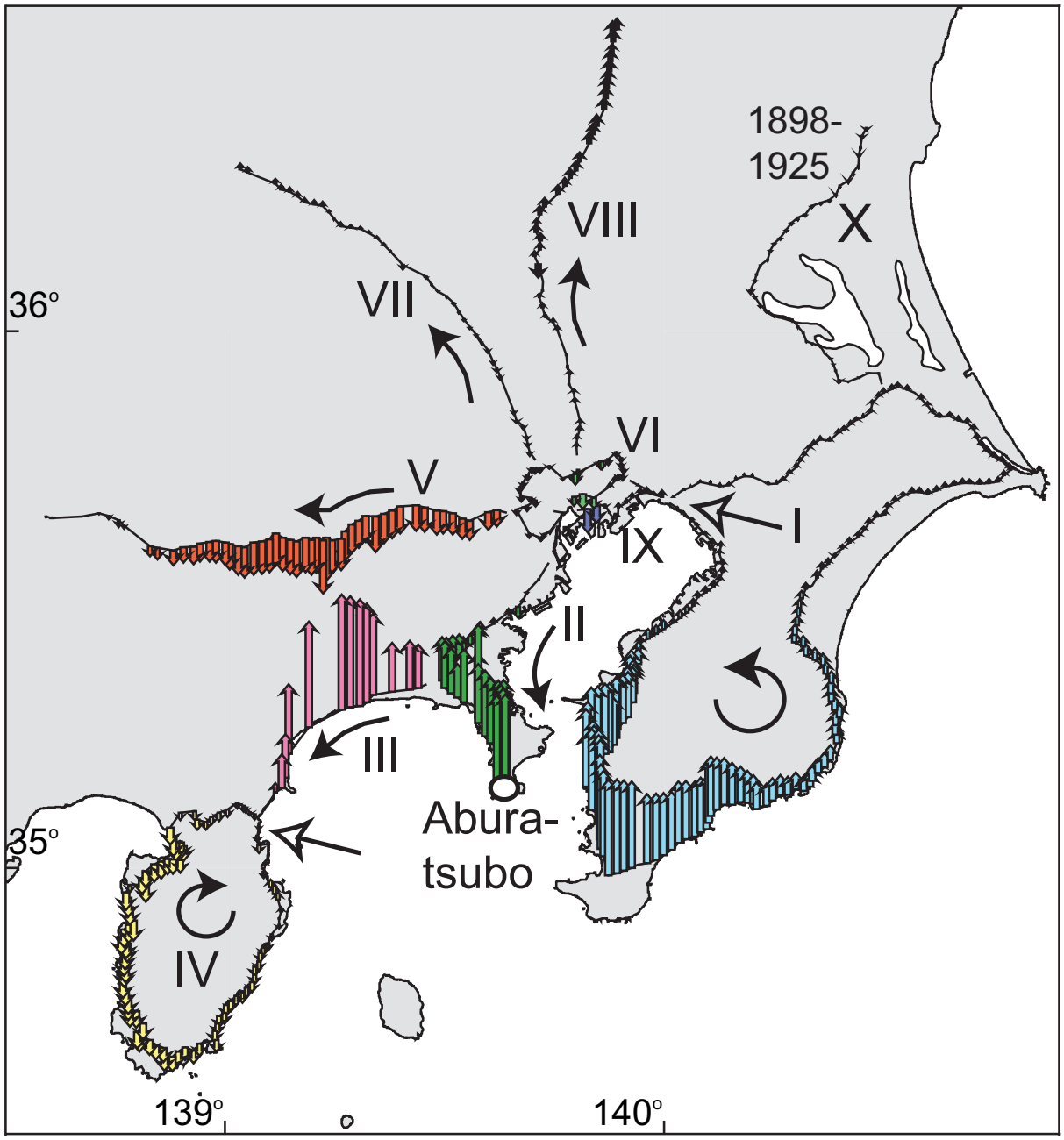

Figure 5. Leveling routes in Kanto and the vertical displacement derived from surveys before and shortly after 1923. The oval indicates tide gage station Aburatsubo that provides the data for the absolute vertical reference frame. The roman enumeration and color coding of the arrows correspond to the profiles shown in Figure 11. The direction in which the profiles in Figure 11 display displacement along the routes is here indicated by a black arrow. For closed loops I and IV the white arrow indicates the start of the profile.

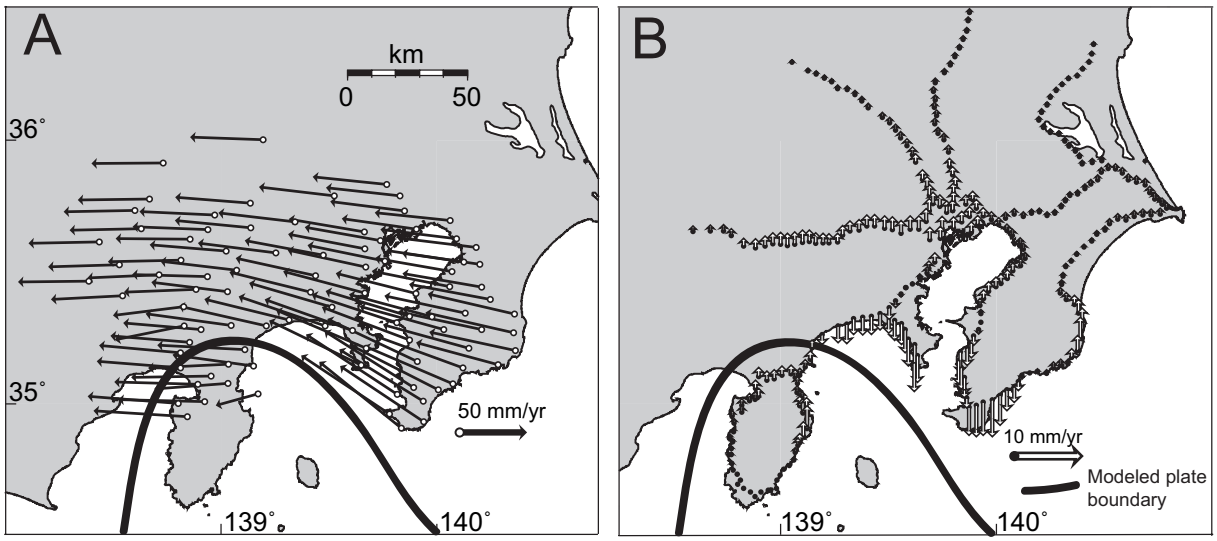

Figure 6. The interseismic velocity field from *Nishimura and Sagiya* [2004] relative to fixed Eurasia. The model is based on continuous GPS data between 1995 and 2000 and produces a velocity field that consists of a rigid plate component and elastic effects caused by the interseismic locking of plates along their interfaces within the boundary zones. A plate interface is parameterized by a multirectangular fault system which accommodates backslip. (A) Horizontal velocity vectors plotted at a selection of the first and second order triangulation bench marks used in this study; (B) Vertical velocities plotted at selected leveling benchmarks.

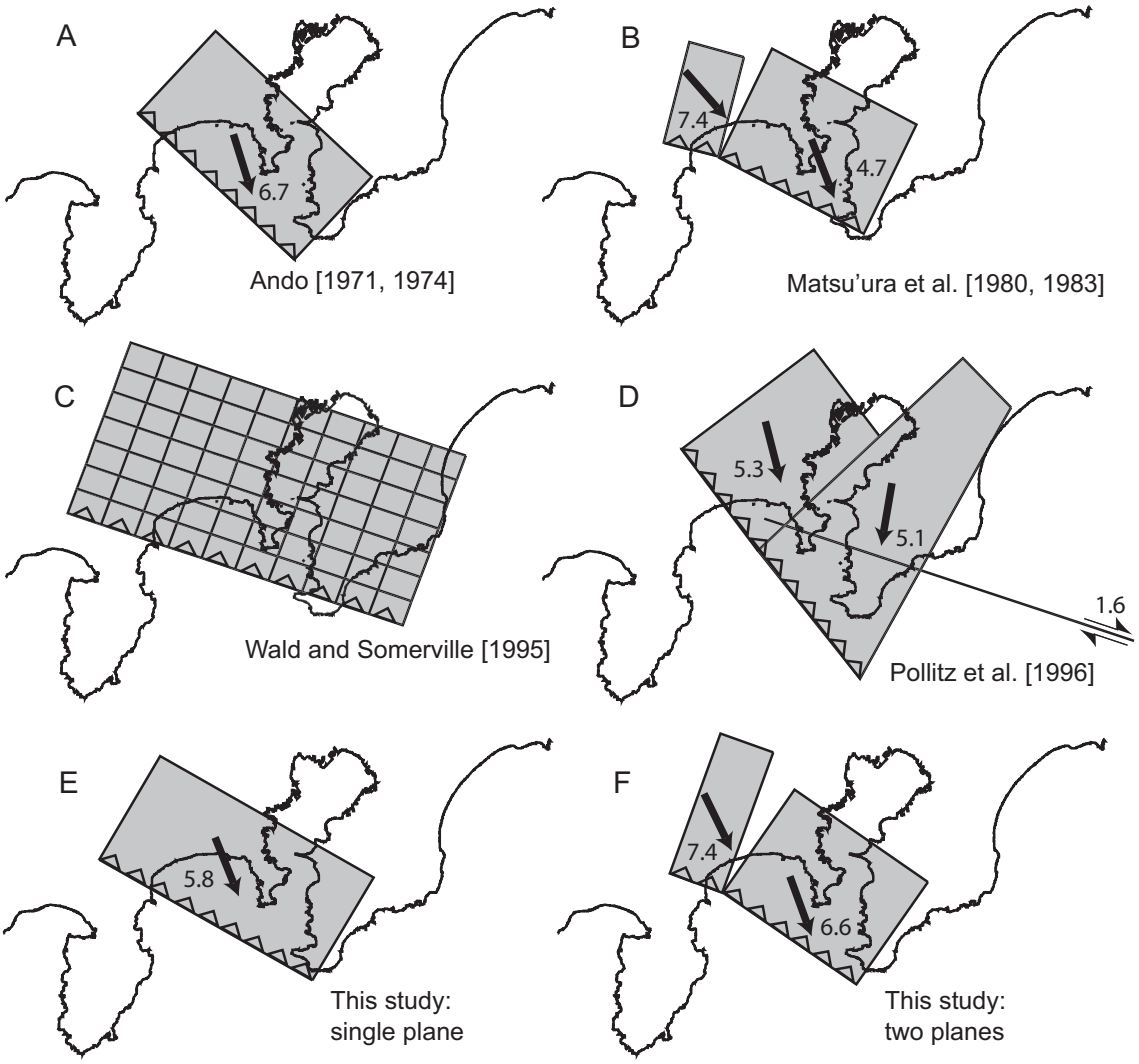

Figure 7. Surface projection of a selection of fault plane models that are based on historical geodetic observations (triangulation and leveling data). The arrows indicate the slip direction, the numbers the magnitude of the slip for the uniform slip models.

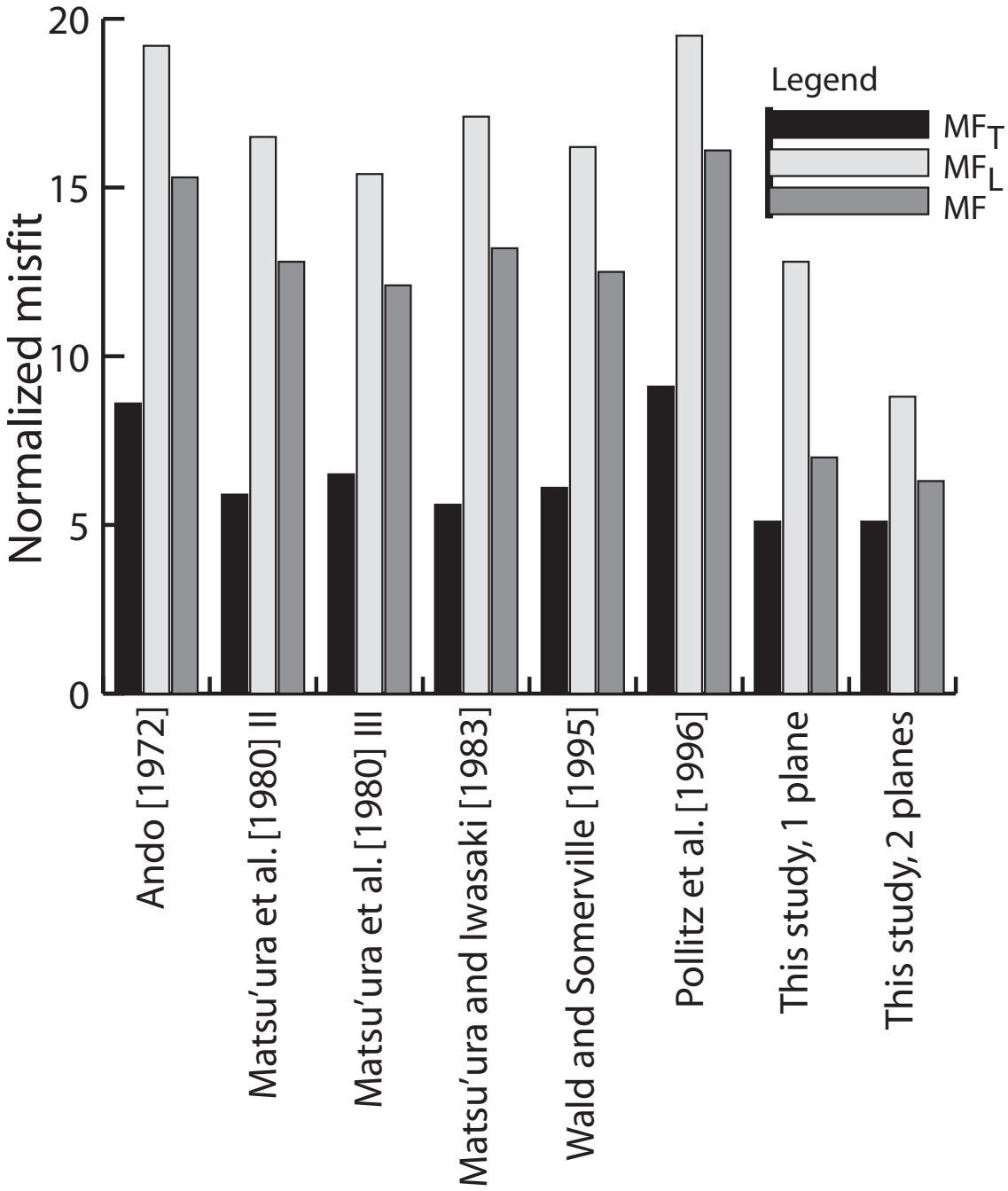

Figure 8. Histogram of normalized root-mean-square (NRMS) misfit values for a selection of fault plane models that are based on historical geodetic observations. MF_T normalized root mean-square (NRMS) misfit (equation 3) between model and triangulation data; MF_L NRMS misfit between model and leveling data; MF NRMS misfit between model and all data.

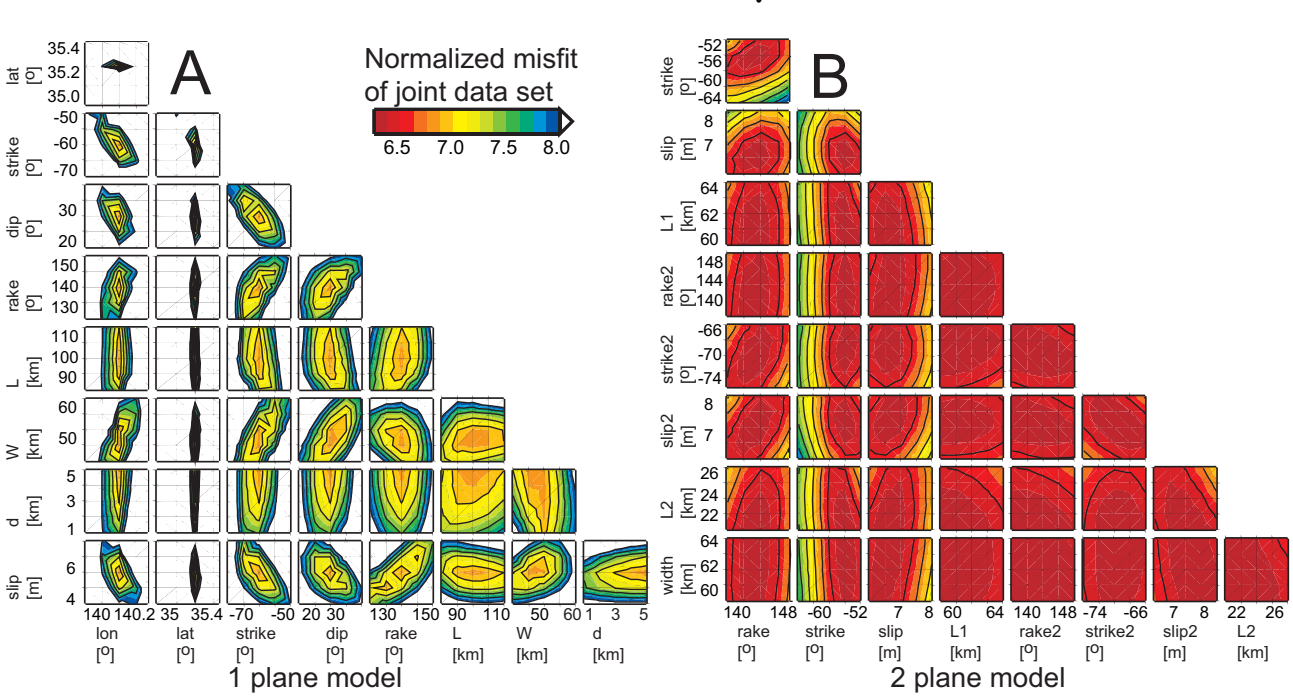

Figure 9. Grid search results for the joint data set (triangulation and leveling data combined). Contoured is the normalized root-mean-square (NRMS) misfit value, defined by equation 3. One block of 36 panels represents all pairwise 2-dimensional neighborhoods (5×5) about the optimal solution projected along the coordinate axis. The values of the optimal model parameters are listed in Table 4. L, W, d denote length, width and buried depth of the upper edge of the fault plane, respectively. (A) Single plane model (solution 1); (B) Two plane model (solution 2). Note that the panels displayed in (A) have different units along the axes than in (B), because the set of model parameters of solution 1 is different from that of solution 2.

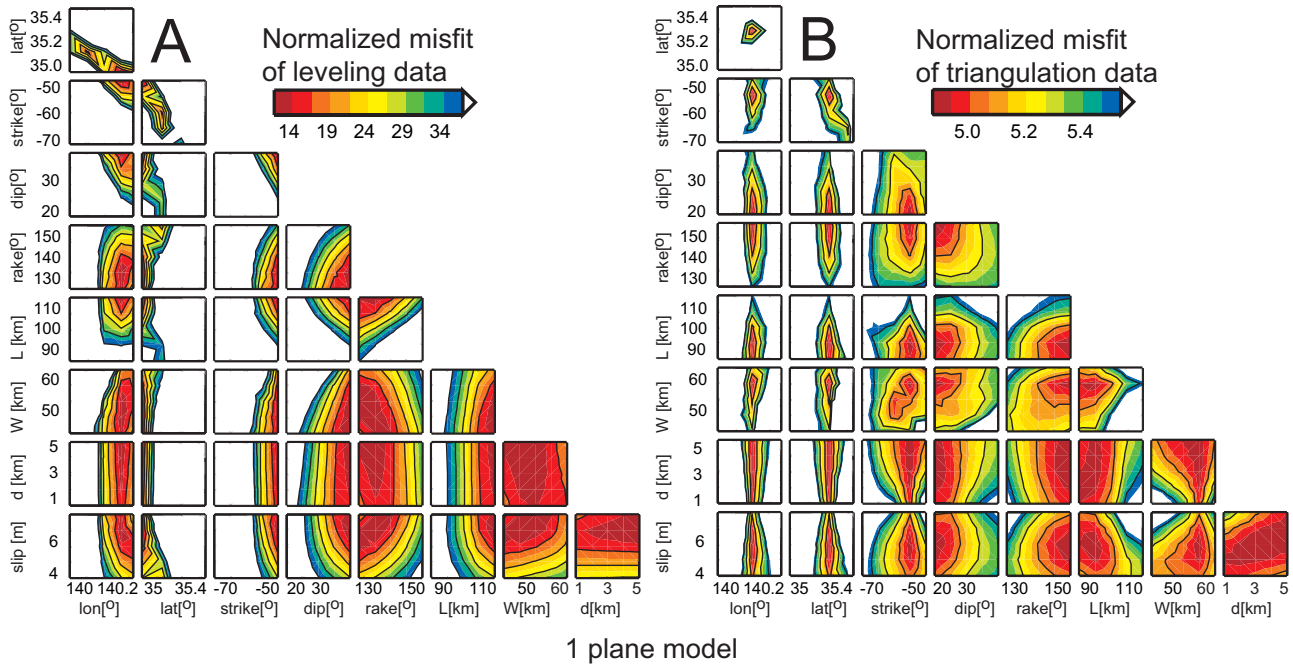

Figure 10. Results of the 9-parameter grid search for the best fitting (optimal) uniform source model consisting of a single fault plane in a uniform half-space for (A) leveling and (B) triangulation data. (The results for the joint data set are shown in Figure 9A). Contoured is the NRMS misfit value, defined by equation 3. See caption of Figure 10 for details.

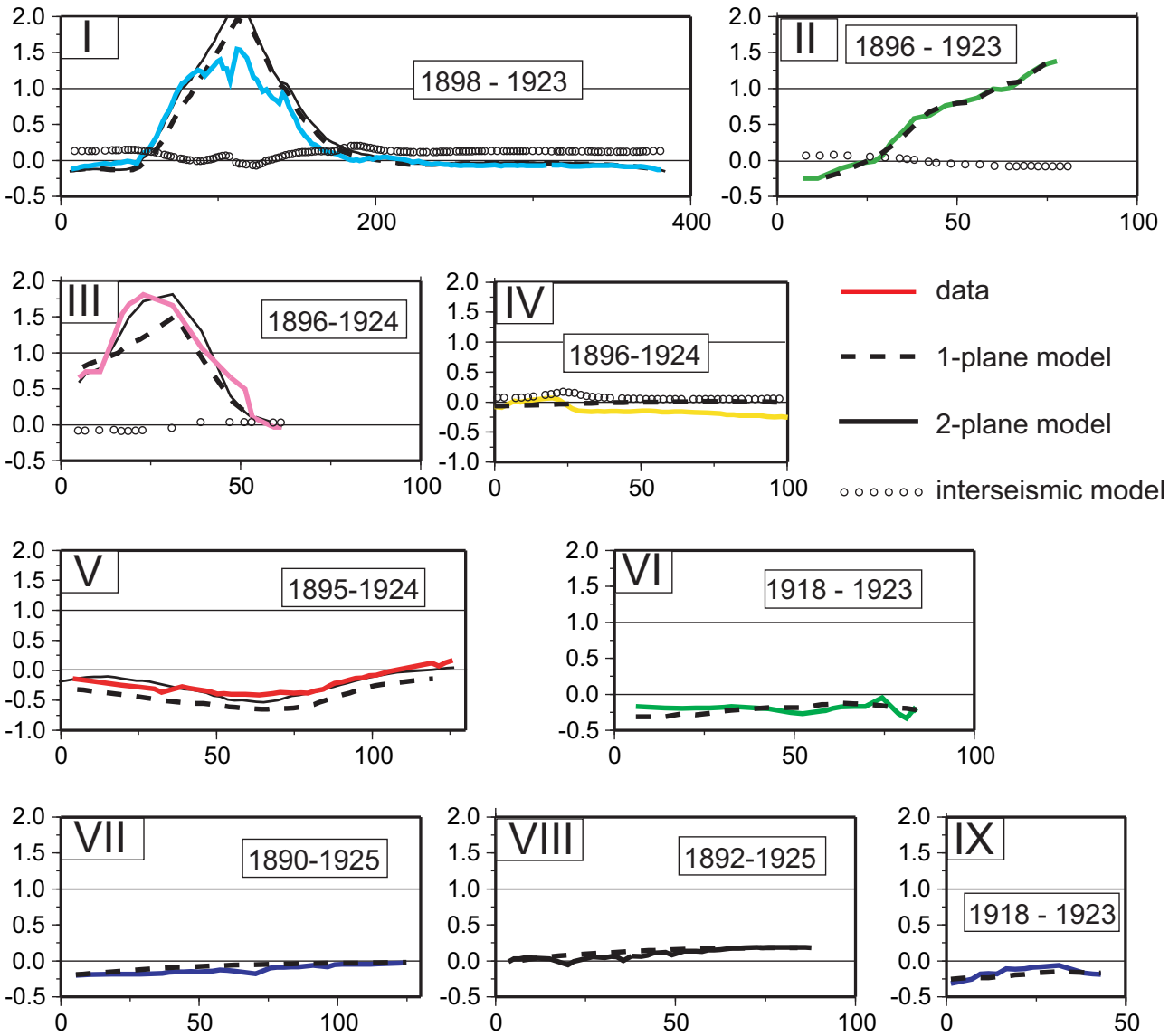

Figure 11. Fit of our uniform source models to the leveling observations that are adjusted for interseismic deformation and indicated by the colored lines. The dashed black lines represent the absolute vertical displacement of our single plane model, the straight black lines represent the double plane model. The color coding and roman numerals correspond to the level routes shown in Figure 5. The vertical component of the interseismic deformation field, plotted for routes I through IV, is omitted for routes V through IX, because there its signal is indistinguishable from zero displacement. Route X (Figure 5) is not displayed here, because the observations do not show any deformation and both models predict zero vertical displacement along this route. The two-plane model curves are not shown for routes II, IV, VI through X, because they are almost identical to the single-plane curves.

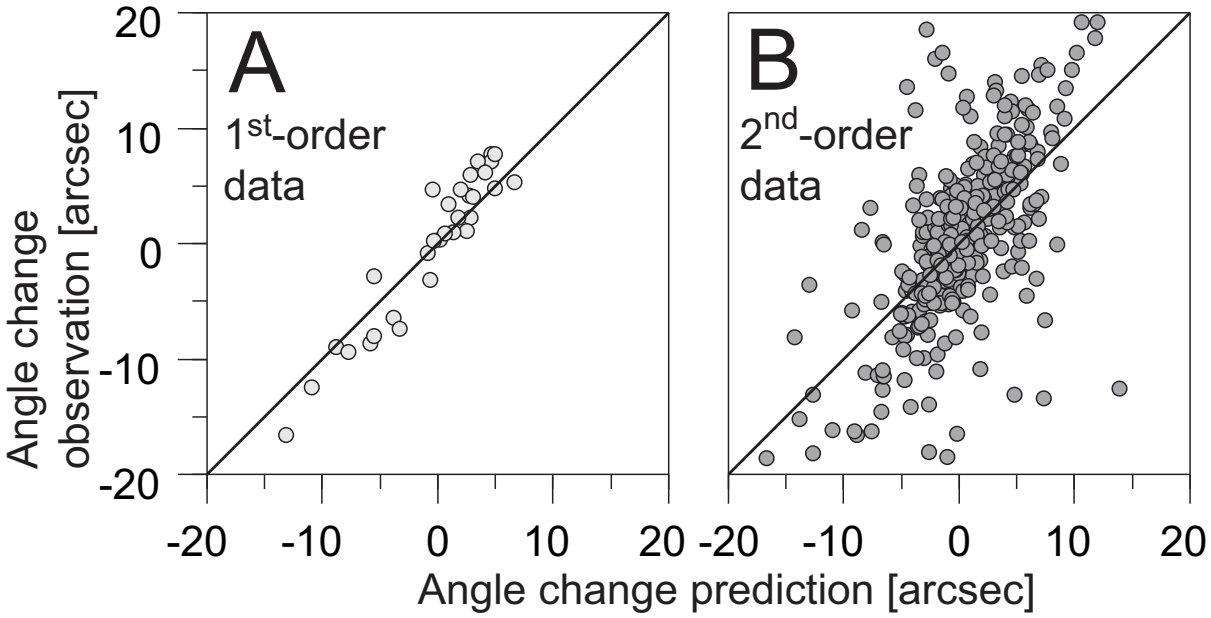

Figure 12. Correlation between predictions by single plane model and first order (A) and second order (B) observations.

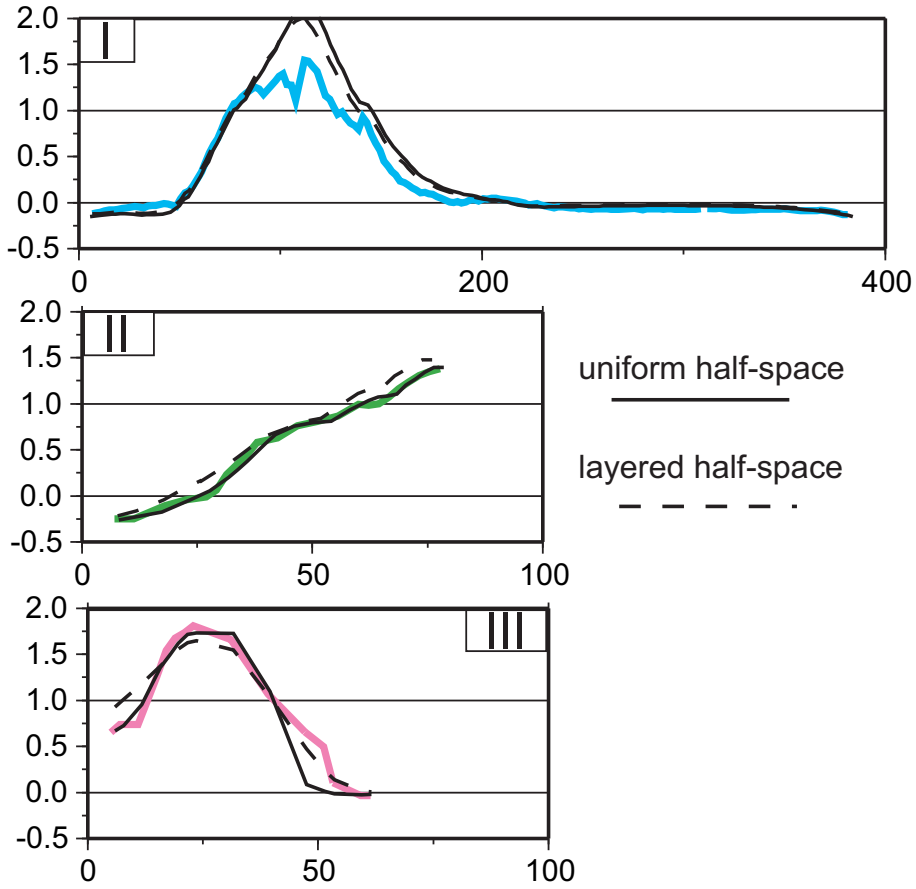

Figure 13. Difference in data fit between the preferred two plane source model in a homogenous half-space and in a layered Earth (Table 5). (A) Only the fit to the leveling data along routes I, II and III changes significantly; (B) Absolute difference in angle change predictions.

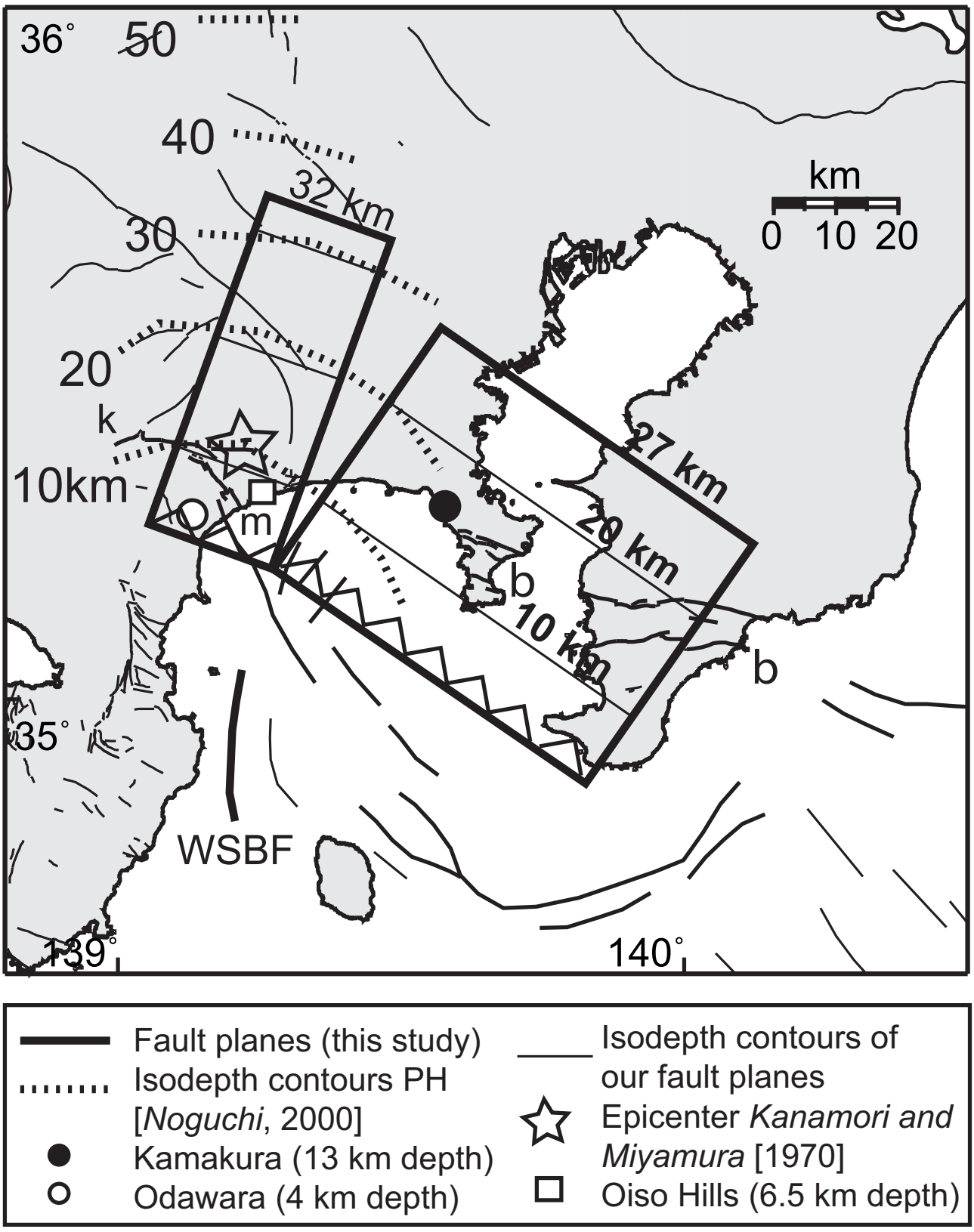

Figure 14. Our two-plane uniform slip source model with isodepth contours for both planes and isodepth contours of the Philippine Sea plate after *Noguchi* [2000]. *k, m, b* indicate the Kannawa, Kozu-Matsuda and Boso transform fault systems, respectively. WSBF Western Sagami Bay Fracture.

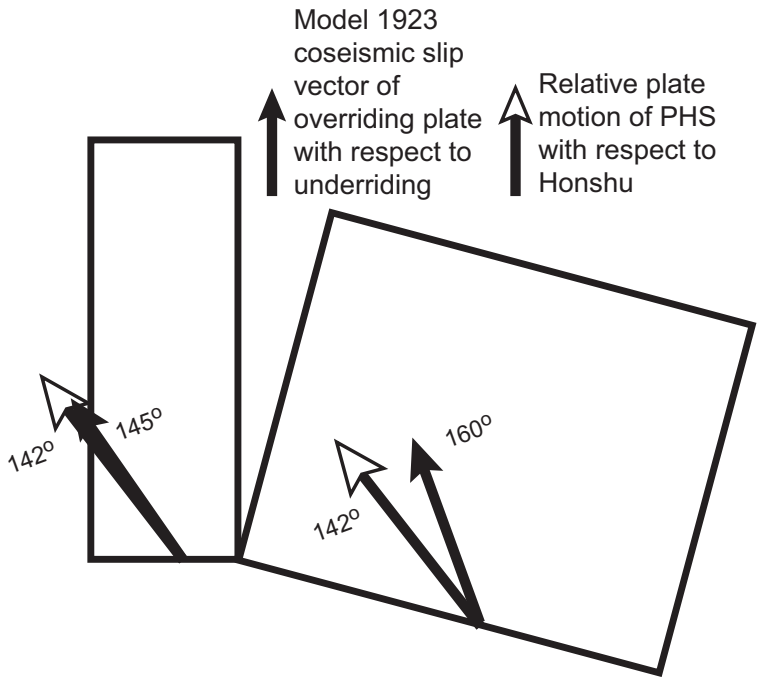

Figure 15. Relative plate motion and resolved slip on the double fault plane model.

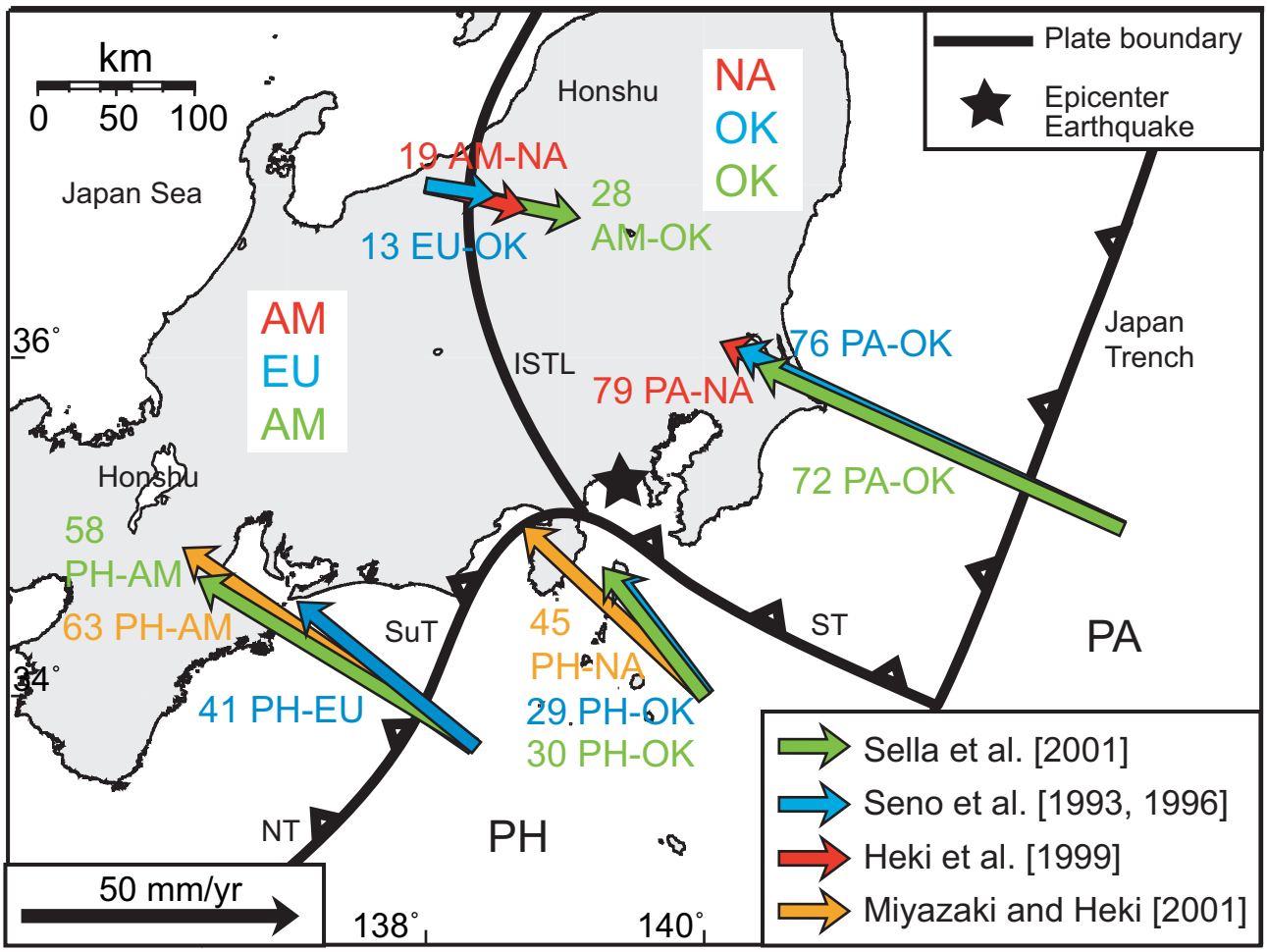

Figure 16. Plate tectonic models for central Japan based on GPS velocity data. Key: AM Amurian, EU Eurasian, NA North American, OK Okhotsk, PA Pacific, PH Philippine Sea plates; ISTL Itoigawa-Shizuoka Tectonic Line, NT Nankai Trough, ST Sagami Trough, SuT Suruga Trough. Arrows show the plate velocities with respect to northern Honshu. Numbers indicate plate velocities in mm/yr, the colors correspond to the colors of the arrows. Velocities shown are the rates predicted by the three main plate models for Japan. In the plate model of *Heki et al.* [1999] and *Miyazaki and Heki* [2001] central and western Honshu are located on the Amurian plate that encompasses eastern Asia and moves independently from the Eurasian plate. This model can explain the regional relative plate motion without the necessity to distinguish the Okhotsk plate from the North American plate. Seno et al. [1993, 1996] postulate the existence of the Okhotsk plate separated from the North American plate along a boundary in Siberia. In this model northeastern Honshu is on the Okhotsk plate and southwestern Honshu is considered as part of Eurasia. *Sella et al.* [2002] use both the Okhotsk and the Amurian plate to describes the plate motion in Japan. The plate codes in the white box refer to the plates distinguished in the three models, the colors correspond to the authors: red for *Heki et al.* [1999] and *Miyazaki and Heki* [2001], blue for *Seno et al.* [1993,1996] and green for *Sella et al.* [2002].

Table 1. Error analysis of the triangulation surveys between 1883 and 1931.

id	Period	Stations *	Closures	δc_{max} ‡ [arcsec]	ϵ_a £ [arcsec]
		first order network			
a	1891-1898	46	44	3.55	0.83
b	1924-1931	37	11	3.06	0.79
a and b	1891-1931	60	55	3.55	0.82
		second order network			
c	1883-1902	1097	694	-10.50	1.23
d	1925-1931	145	79	6.43	1.31
c and d	1883-1931	1136	773	-10.50	1.23

* Number of stations that contributes to closures

¶ Signal-to-noise ratio

‡ Largest closure (equation 1) found in the particular data subset.

£ Average observation error (equation 2).

Table 2. Components of the geodetic data set used in this study.

Bench marks	Data	Preseismic survey	Postseismic survey	SNR ¶
		1^{st} order triangulation		
15	31	1891-1898	1924-1925	7.86
		2^{nd} order triangulation		
178	435	1883-1900	1924-1925	5.67
		1^{st} and 2^{nd} order triangulation combined		
193	466	1883-1900	1924-1925	5.88
		leveling		
469	469	1898-1918	1923-1925	43.78

¶ Signal-to-noise ratio

Table 3. Estimates of leveling errors averaged over periods 1884-1923 and 1923-40.

Year	1884	'92	'95	'98	1902	'09	'18	'24	'25	'29	'30	'34	'37	'38	'42
# †	77	56	54	63	60	51	73	213	40	44	58	40	118	152	76
α [mm/km] §	1.55	0.61	0.60	0.50	0.53	0.55	0.46	0.63	0.53	0.53	0.50	0.69	0.56	0.72	0.63
$\widetilde{\alpha}$ [mm/km] ‡	1.55	0.54						0.62							

† Number of randomly chosen double-run leveling sections that contribute to α.

§ Observed average leveling error per year normalized to a distance of 1 km.

‡ Assigned average leveling error per multiple year period normalized to a distance of 1 km.

Table 4. Comparison of source models of the 1923 Kanto earthquake, based on geodetic data.

Strike[a]	Dip	Rake	Length[b] [km]	Width[c] [km]	Lon[d]	Lat[d]	Depth[e] [km]	Slip[f] [m]	Slip azimuth[g]	MF_T[h]	MF_L[i]	MF[j]	dof[k]
						Ando [1974]							
-45°	30°	153°	85	55	140.1°E	35.1°N	0.0	6.7	162°	8.6	19.2	15.3	9
						Matsu'ura et al. [1980], *model II*							
-66°	25°	140°	95	54	140.1°E	35.3°N	1.9	4.8	154°	5.9	16.5	12.8	9
						Matsu'ura et al. [1980], *model III*							
-64°	23°	138°	63	55	140.1°E	35.3°N	1.5	4.7	158°	6.5	15.4	12.1	15
-75°	26°	147°	22	45	139.4°E	35.5°N	1.5	7.4	138°				
						Matsu'ura and Iwasaki [1983]							
-67°	26°	142°	93	53	140.1°E	35.3°N	2	4.6	151°	5.6	17.1	13.2	9
						Wald and Somerville [1995]							
-70°	25°	90-180°[l]	130	70	139.5°E[m]	35.0°N[m]	2.0	0-7.8°[o]	110°-200°[n]	6.1	16.2	12.5	140
						Pollitz et al. [1996]							
-39°	38°	156°	41	74	139.9°E	35.4°N	0.3	5.3	165°	9.1	19.5	16.1	25
-68°	90°	180°	130	12	140.8°E	35.8°N	0.3	1.6	112°				
-39°	20°	132°	75[p]	116	140.5°E	35.5°N	0.3	5.1	189°				
						This study, one fault plane, best fit to leveling data							
-50°	39°	134°	113	46	140.283°E	34.884°N	5.0	6.8	176°	5.6	11.1	7.1	9
						This study, one fault plane, best fit to triangulation data							
-55°	19°	150°	91	56	140.128°E	35.202°N	4.0	5.8	148°	4.9	32.2	9.3	9
						This study, one fault plane, best fit to combined data							
-60°	**27°**	**142°**	**99**	**46**	**140.128°E**	**35.202°N**	**3.0**	**5.8**	**158°**	**5.1**	**12.8**	**7.0**	**9**
						This study, two fault planes, best fit to leveling data							
-52°	27°[q]	148°	61	53[q]	140.122°E[q]	35.225°N[q]	3.0[q]	6.6	160°	5.2	8.3	6.3	14
-60°	27°[q]	133°	21	64	139.526°E	35.695°N	3.0[q]	7.4	167°				
						This study, two fault planes, best fit to triangulation data							
-58°	27°[q]	145°	61	53[q]	140.122°E[q]	35.225°N[q]	3.0[q]	8.1	157°	4.9	14.7	6.9	14
-68°	27°[q]	145°	24	64	139.509°E	35.632°N	3.0[q]	6.4	147°				
						This study, two fault planes, best fit to combined data							
-55°	**27°**[q]	**145°**	**61**	**53**[q]	**140.122°E**[q]	**35.225°N**[q]	**3.0**[q]	**6.6**	**160**	**5.1**	**8.8**	**6.3**	**14**
-70°	**27°**[q]	**145°**	**22**	**64**	**139.480°E**	**35.666°N**	**3.0**[q]	**7.4**	**145**				

[a] In the definition of the fault plane geometry we adopt *Okada's* [1985] convention, where the z-axis of our coordinate system points upwards (i.e. out of the Earth) and the strike of the fault plane is parallel to the x-axis.

[b] Length of fault plane along its strike.

[c] Downdip width of fault plane

[d] Coordinates of the vertical projection onto the Earth's surface of the easternmost corner of the lower edge of the fault plane.

[e] Buried depth of upper edge of the fault plane.

[f] The slip vector represents the movement of the hanging-wall block with respect to the foot-wall block.

[g] Direction of slip in horizontal plane.

[h] Normalized root mean-square (NRMS) misfit (equation 3) between model and triangulation data.

[i] NRMS misfit between model and leveling data.

[j] NRMS misfit between model and all data.

[k] Number of degrees of freedom.

[l] Rake varies between right lateral and reverse slip.

[m] Coordinates of center of upper edge of fault plane.

[n] Slip direction varies between SSW and SE.

[o] Average slip is 3.5 m, maximum slip is 7.8 m.

[p] Trapezoidal fault plane.

[q] Value is kept fixed in grid search.

Table 5. Velocity structure model for Kanto from *Takeo and Kanamori* [1992].

Depth[a] (km)	Thickness (km)	V_p (km/sec)	V_s (km/sec)	ρ (g/cc)
0.0[b]	*1.0*[b]	*1.83*[b]	*0.7*[b]	*2.0*[b]
1.0	1.7	2.8	1.3	2.3
2.7	3.4	5.6	2.9	2.5
6.1	12.9	6.0	3.4	2.6
19.0	-	6.8	4.0	3.0

[a] Depth to the top of the layer.

[b] The soft sedimentary layer characteristic for the Kanto plain.